



Investigating the vaporization mechanism's effect on interfacial tension during gas injection into an oil reservoir

Hossein Mehrjoo¹ · Ali Safaei² · Yousef Kazemzadeh³ · Masoud Riazi⁴ · Atefe Hasan-zadeh⁵

Received: 18 July 2023 / Accepted: 10 May 2024 / Published online: 4 June 2024
© The Author(s) 2024

Abstract

In gas injection, which is one of the fascinating enhanced oil recovery techniques, the main mechanism involves decreasing interfacial tension (IFT). Although various mechanisms can affect the IFT of a system, in most experimental and numerical studies, condensation is considered the dominant mechanism among condensation-vaporization and vaporization. Investigating the impact of each mechanism is crucial as they can influence the IFT of the system and, consequently, the effectiveness of the gas injection method. This study introduces a novel model to assess the influence of different mechanisms on system IFT. The model defines system IFT, adjusts fluid relative permeability to represent miscible, immiscible, and near-miscible states, and utilizes the Buckley–Leverett method to analyze gas fractional flow and saturation profiles when injecting carbon dioxide (CO₂), methane (CH₄), and nitrogen (N₂). Furthermore, the research explores the impact of injection pressure and IFT at minimum miscible pressure (IFT₀) on gas injection efficiency. Based on our results, for both live and dead oil, the condensation mechanism reduces IFT and near-miscible pressure; switching to a condensing-vaporizing mechanism increases these parameters. This trend was consistent across all gases studied (N₂, CO₂, CH₄), with a more significant effect observed on the CH₄-live oil system compared to N₂ and CO₂. Controlling the condensing mechanism in IFT measurements enhances gas flow rate and relative permeability curve within the medium. Higher injection pressure in the condensing mechanism and IFT₀=0.5 leads to faster fluid movement and improved relative permeability due to increased driving forces. Higher IFT₀ accelerates the relative permeability of fluids and gas movement within the medium by promoting miscibility sooner. The impact of IFT₀ was more pronounced on the dead oil–gas system compared to the live oil–gas system in this study.

Keywords Gas injection · Vaporized oil in gas phase · Relative permeability · Saturation profile · Interfacial tension

List of symbols

Greek letters

γ_{API}	American Petroleum Institute
γ_g	Specific gravity of gas
γ_o	Specific gravity of oil
μ_g	Gas viscosity (mPa.s)
$\mu_{g\text{eff}}$	Gas effective viscosity (mPa.s)
μ_o	Oil viscosity (mPa.s)
$\mu_{o\text{eff}}$	Oil effective viscosity (mPa.s)
ρ_g	Density of gas phase $\left(\frac{\text{lbm}}{\text{ft}^3}\right)$
ρ_o	Density of oil phase $\left(\frac{\text{lbm}}{\text{ft}^3}\right)$
σ	IFT at different pressure $\left(\frac{\text{dynes}}{\text{cm}}\right)$
σ_0	IFT at MMP $\left(\frac{\text{dynes}}{\text{cm}}\right)$
σ_{go}	IFT of gas and oil $\left(\frac{\text{dynes}}{\text{cm}}\right)$
ϕ	Porosity (%)
ω	Mixing factor

✉ Yousef Kazemzadeh
yusefkazemzade@yahoo.com; yusefkazemzade@pgu.ac.ir

✉ Masoud Riazi
mriazi180@gmail.com; masoud.riazi@nu.edu.kz

¹ Department of Petroleum Engineering, Shahid Bahonar University of Kerman, Kerman, Iran

² Department of Petroleum Engineering, College of Engineering, University of Tehran, Tehran, Iran

³ Department of Petroleum Engineering, Faculty of Petroleum, Gas, and Petrochemical Engineering, Persian Gulf University, Bushehr, Iran

⁴ School of Mining and Geosciences, Nazarbayev University, Astana, Kazakhstan

⁵ Fouman Faculty of Engineering, College of Engineering, University of Tehran, P.O.Box 43581-39115, Guilan, Iran

Latin letters

A-F	Brill and Beggs' constant for calculation of compressibility factors
Area	Cross section area (m ²)
B_o	Oil formation volume factor $\left(\frac{\text{bbl}}{\text{STB}}\right)$
CO ₂	Carbon dioxide
CH ₄	Methane
$\frac{df_g}{dS_g}$	Derivative of the fractional flow of gas phase to gas saturation
f_g	Fractional flow of gas
F_k	Relative permeability interpolation parameter
K_{RG}	Gas relative permeability
K_{rg}	Gas relative permeability at residual oil saturation
K_{rg}^{imm}	Immiscible gas relative permeability
K_{rg}^{mis}	Miscible gas relative permeability
K_{RO}	Oil relative permeability
K_{ro}	Oil relative permeability at irreducible gas saturation
K_{ro}^{imm}	Immiscible oil relative permeability
K_{ro}^{mis}	Miscible oil relative permeability
L	Length of domain (m)
M_g	Molecular weight of gas phase $\left(\frac{\text{lbm}}{\text{lbmol}}\right)$
M_{go}	Average molecular weight of gas phase $\left(\frac{\text{lbm}}{\text{lbmol}}\right)$
M_o	Molecular weight of oil phase $\left(\frac{\text{lbm}}{\text{lbmol}}\right)$
M_{og}	Average molecular weight of oil phase $\left(\frac{\text{lbm}}{\text{lbmol}}\right)$
N	The inverse of read-in-exponent
N_2	Nitrogen
n_g	Gas exponent for Brooks–Corey functions
n_l	Read-in exponent
n_m	Relative permeability index
n_o	Oil exponent for Brooks–Corey functions
P	Pressure (psia)
P_g	Parachor equation for gas phase
P_o	Parachor equation for oil phase
P_{pc}	Pseudocritical temperature (psia)
P_{pr}	Pseudoreduced pressure
PVI	Dimensionless pore volume
q_t	Total injection rate $\left(\frac{\text{m}^3}{\text{hr}}\right)$
R_s	Solution gas oil ratio $\left(\frac{\text{scf}}{\text{STB}}\right)$
r_v	Vaporized oil in the gas phase $\left(\frac{\text{scf}}{\text{STB}}\right)$
S_g	Gas saturation
S_{gi}	Irreducible gas phase saturation
S_{gi}^{imm}	Irreducible gas phase saturation at the immiscible condition
S_o	Oil saturation
S_{or}	Residual oil saturation

S_{or}^{imm}	Residual oil saturation at the immiscible condition
t	Injection time (hr)
T	Temperature (R)
T_{pc}	Pseudocritical temperature (R)
T_{pr}	Pseudoreduced temperature
V	Viscosity ratio
x_g	Mole fraction of gas in the oil phase
x_o	Mole fraction of oil in the oil phase
x_{S_g}	Distance moved by a specific S_g contour (m)
y_g	Mole fraction of gas in the gas phase
y_o	Mole fraction of oil in the gas phase
Z	Compressibility factor

Abbreviations

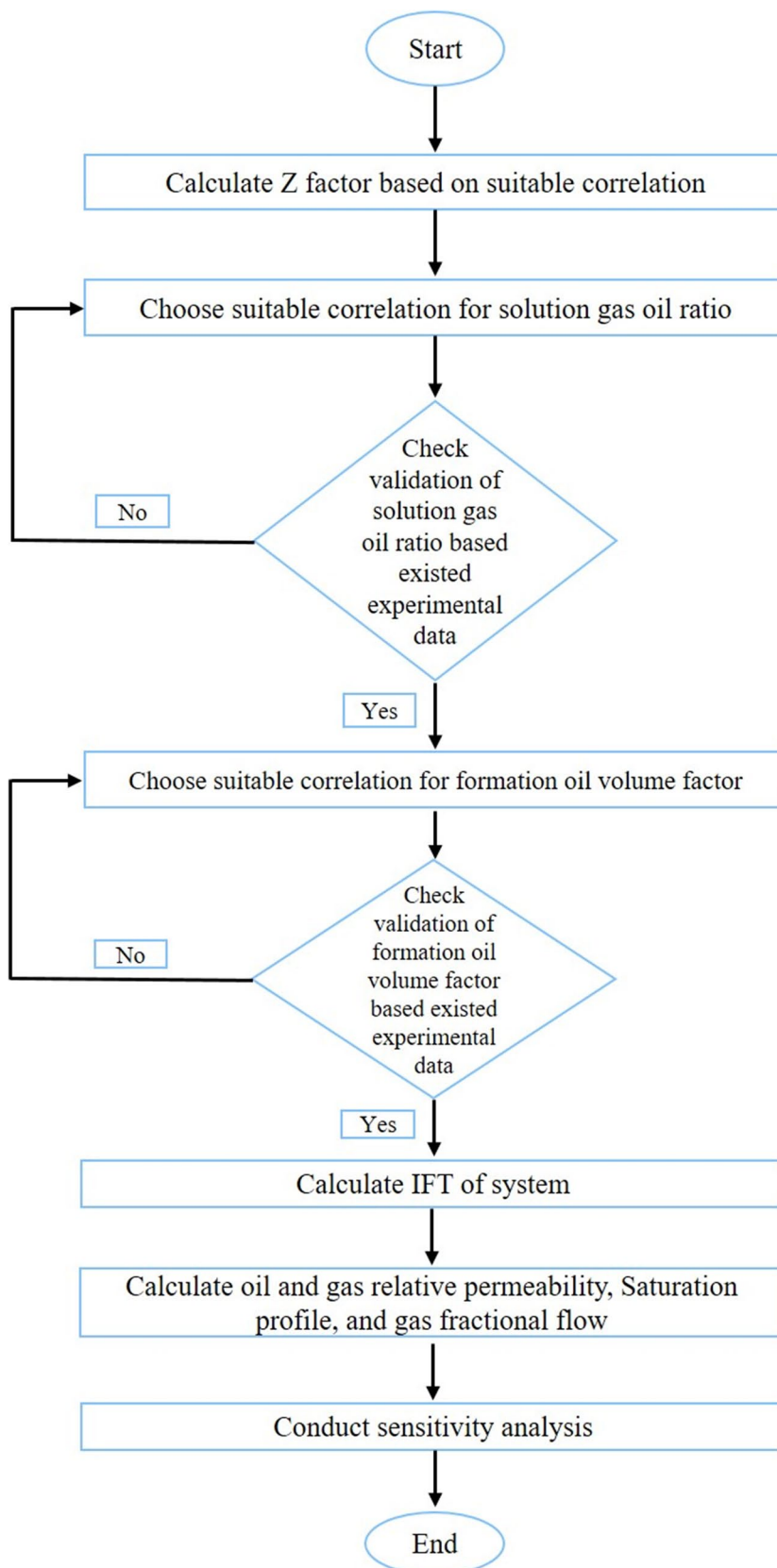
EOR	Enhanced oil recovery
IFT	Interfacial tension
MMP	Minimum miscibility pressure
SWAG	Simultaneous gas and water
WAG	Water alternating-gas

Introduction

The traditional approach fails to retrieve around 60–70% of the oil reserves. On the other hand, the growth in population has resulted in an increase in the need for energy resources. Therefore, Enhanced Oil Recovery (EOR) has emerged as a crucial technique to sustain oil production levels and retrieve extra oil from reservoirs. Based on the type of oil, reservoir characteristics, and other factors, various classifications have been introduced for EOR methods in the literature, including thermal, gas injection, chemical injection, microbial, electromagnetic heating, etc. For example, thermal methods are more suitable for heavy oil (Wu et al. 2018, 2016). Among the introduced EOR methods, gas injection, which can be injected under three conditions—miscible, immiscible, and near-miscible, has attracted significant attention. Therefore, many researchers have explored this technique both numerically and experimentally to expand understanding of this approach.

Kulkarni and Rao (2005) assessed the effectiveness of water alternating-gas (WAG) injection in both miscible and immiscible scenarios. According to their findings, superior results were observed in the miscible conditions. Karima et al. (2007) investigated the injection of secondary and tertiary gases into fractured carbonate rock. Their findings showed that carbon dioxide (CO₂) is more efficient than nitrogen (N₂) in improving oil recovery. Ghafouri et al. (2012) conducted a study on injecting WAG, N₂, and CO₂ gases into a carbonate reservoir. Their findings indicated that decreased gas injection resulted in higher oil production. Sohrabi and Fatemi (2012) investigated oil recovery

Fig. 1 The Flow chart of the numerical simulation



during gas, water, WAG, and simultaneous gas and water (SWAG) injections. Their research indicated that WAG resulted in superior oil recovery outcomes among the various injection methods. Fatemi and Sohrabi (2013) carried out several experiments to explore how rock wettability influences oil recovery in gas injection, water injection, and WAG injection, in a separate study. Shahrokhi et al. (2018) carried out a sequence of core flood experiments to examine how injection history and miscibility influence oil recovery when employing gas injection. They showed that using water flooding in mixed-wet carbonate formations resulted in better outcomes compared to immiscible gas injection. Additionally, they noted that the residual oil saturation after immiscible WAG following gas injection was higher than after water flooding. Their research indicated that the injection order did not affect the final oil recovery. Gas injection is a promising method for EOR in unconventional reservoirs, as well as in conventional reservoirs. In addition to the studies mentioned above, numerous researchers have explored different gas injection techniques, including gas flooding and cyclic gas injection, through experimental and numerical methods, as well as field studies (Chen et al. 2014; Fathi and Akkutlu 2014; Gamadi et al. 2014; Hoffman 2012; Jin et al. 2017a, b; Jin et al. 2017; Li and Sheng 2017; Meng et al. 2017; Sanchez-Rivera et al. 2015; Sheng and Chen 2014; Sun et al. 2016; Yu et al. 2015, 2017). In the process of gas injection, our goal is to minimize the Interfacial Tension (IFT) as much as possible to enhance oil recovery (Jin 2017). In other words, the primary mechanism of gas injection is the reduction of interfacial IFT; therefore, it is essential to investigate the IFT of gas-oil. This has resulted in the conduct of various studies to examine the IFT between gas and different fluid systems in diverse conditions.

In many reservoir engineering investigations, knowledge of the system's IFT is essential as it impacts fluid flow (Shariat 2014). About one-third of the oil reserves might not be recoverable because of the interfacial tension of the system (Jennings and Newman 1971). A low IFT leads to a decrease in residual oil saturation (Harbert 1983). This reduction in IFT can also impact the shape of the relative permeability curve. When the IFT approaches zero, both residual oil saturation and the relative permeability curve become linear (Shariat 2014). The assessment of the IFT in gas injection processes has sparked considerable interest as the varying strengths of viscous, gravitational, and surface forces play a crucial role in determining the ultimate reservoir recovery potential (Shariat 2014). Many researchers have studied the IFT between gas and water at different temperature and pressure levels (Akutsu et al. 2007; Bennion and Bachu 2008; Chen and Yang 2019; Chiquet et al. 2007; Chun and Wilkinson 1995; Da Rocha et al. 1999; Hebach et al. 2002; Heuer JR 1957; Hocott 1939; Hough et al. 1951; Jaeger 1998; Jennings and Newman 1971; Jho et al. 1978; Kashefi 2012; Lepski 1997; Massoudi and King Jr 1975;

Mehrjoo et al. 2020; Ren et al. 2000; Rushing et al. 2008; Sachs and Meyn 1995; Shariat 2014; Sutjiadi-Sia et al. 2008; Tewes and Boury 2004; Wiegand and Franck 1994; Yang et al. 2005; Yiling et al. 1997; Zhao et al. 2002). The study conducted by Escrochi et al. (2013) investigated the IFT behavior of gas and oil when gas is injected into asphaltene-containing oil. They showed that as the pressure increased, the likelihood of achieving miscibility also increased near the point where asphaltene precipitation begins (Escrochi et al. 2013). Dalvand and Heydarian (2015) conducted a study where they measured the IFT of gas oil for two Iranian oil formations. They highlighted a significant impact of temperature on the IFT. Ghorbani and Mohammadi (2017) conducted a study on the effect of pressure, fluid composition, and temperature on the IFT of oil–gas systems. They employed the pendant drop technique for measurement and analyzed the images using the Axisymmetric Drop Shape Analysis method. Their research revealed that the influence of pressure on IFT was more significant compared to the effect of temperature. Additionally, they illustrated that the composition's impact on IFT is determined by the phase envelope of the sample. Jahabakhsh et al. (2018) examined how reducing gas–oil IFT affects three-phase relative permeability. In addition to experimental research, certain studies prediction the IFT of gas-oil and gas–water systems (Ahmadi and Mahmoudi 2016; Chen and Yang 2019; Kashefi 2012; Kashefi et al. 2016; Mehrjoo et al. 2020; Shariat 2014).

Although multiple studies have aimed to elucidate the behavior and mechanism of gas injection processes in EOR, numerous questions persist regarding this method. While most experimental and numerical analyses emphasize the

Table 1 Parameters for simulation of IFT and gas injection

Inputs parameters	Value
Reservoir temperature (T_{res})	643.77 R
Gas viscosity (μ_g)	0.035 mPa.s
Oil viscosity (μ_o)	1.81 mPa.s
Length of the simulated domain (L)	200 m
API of reservoir oil (API)	19.96
Bubble point pressure (P_b)	1379 psi
Gas relative permeability at residual oil saturation (KRG)	0.6181
Oil relative permeability at irreducible gas saturation (KRO)	0.9
Initial saturation of gas (S_{gi})	0.05
Initial saturation of oil (S_{oi})	0.95
Residual oil saturation (S_{or})	0.24
φ	0.2
k	20 md
N	$\frac{1}{4}$
n_g	2.9852
n_o	2.1079

prevalence of the condensing mechanism, the impact of the vaporizing mechanism on the IFT and the efficiency of gas injection remains ambiguous, necessitating additional research. Therefore, in the first step of this study, the IFT of different gas systems (nitrogen, carbon dioxide, methane) and oil during various mechanisms has been investigated. Since the IFT of systems can affect the gas injection process, the second step of the study focused on examining the effect of vaporized oil in the gas phase, injection pressure, and IFT on the model's output, namely the relative permeability of fluids, saturation profile of gas, and fractional flow curve.

After the introduction, the mathematical model is described in Sect. 2. Section 3 covers the validation of the developed code, results, discussion, and sensitivity analysis of the parameters considered, followed by some concluding remarks.

Method of work

Mathematical model

Figure 1 shows the flow chart of the present research. The mathematical model in this article includes four primary stages: determining the IFT of the system, adjusting the relative permeability of gas and oil, computing the saturation profile, and identifying the gas fractional flow as the model's result (Fig. 1).

Calculation of IFT

IFT plays a crucial role in influencing the behavior of reservoir fluids. Lowering the IFT is a key factor in enhanced oil recovery EOR techniques like gas injection. The determination of IFT can be done either through experimental measurements or simulation approaches. Various correlations have been proposed by researchers to estimate the IFT

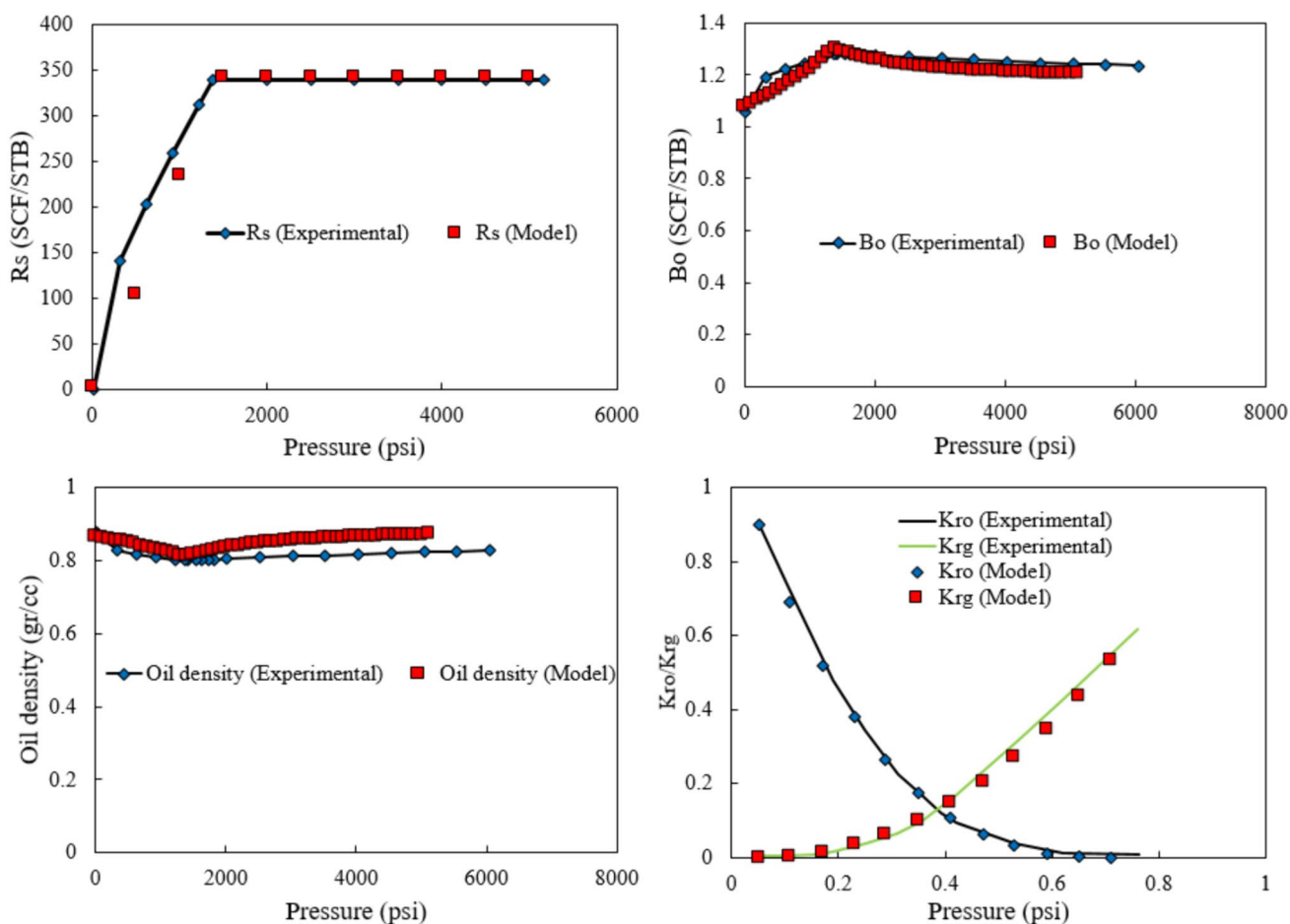


Fig. 2 Comparison of the experimental data and predicted data for solution gas oil ratio, oil formation volume factor, oil density, and oil and gas relative permeability

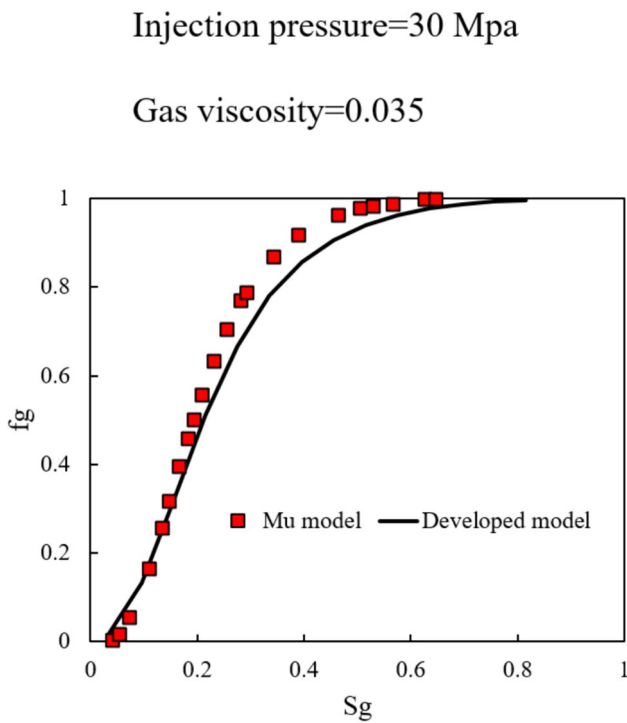


Fig. 3 Comparison predicted fractional flow of Mu et al. (2019) and present paper with at gas viscosity of 0.035 mPa.s and injection pressure of 30 MPa

of a system, with the Ramey correlation, derived from the Weinaug–Katz correlation, being widely recognized (Ramey Jr 1973). In this study, the Ramey correlation was employed to calculate the IFT of the gas–oil system.

$$\sigma_{go}^{1/4} = P_o \left(x_o \frac{\rho_o}{M_{og}} - y_o \frac{\rho_g}{M_{go}} \right) - P_g \left(x_g \frac{\rho_o}{M_{og}} - y_g \frac{\rho_g}{M_{go}} \right) \tag{1}$$

In the given equation, ρ_g , x_g , y_g , and M_{go} correspond to the gas density, gas mole fraction in the oil phase, gas mole fraction in the gas phase, and gas molecular weight, respectively. Likewise, ρ_o , x_o , y_o , and M_{og} , represent the oil density, oil mole fraction in the oil phase, oil mole fraction in the gas phase, and oil molecular weight, respectively. Furthermore, σ_{go} stands for the IFT of the oil and gas system, while P_o and P_g are Parachor equations for the oil and gas phases. The formulas for computing the aforementioned parameters and other relevant parameters are detailed in Eqs. (22) to (48) in the appendix.

Calculation of relative permeability of the oil–gas system

In the second step of the algorithm developed in this study, the relative permeability was adjusted to account for both immiscible and miscible conditions. Various models have been proposed by researchers to modify the relative

permeability, aiming to interpolate between these two conditions. One well-known model utilized in this study is the one put forth by Coats (1980). The parameter introduced to interpolate between immiscible and miscible conditions is the relative permeability interpolation parameter, F_k , which is linked to IFT and the IFT at minimum miscibility pressure (MMP), IFT0. The formulation for F_k is presented in the following equation:

$$F_K = \min \left[1, \left(\frac{\sigma}{\sigma_0} \right)^N \right] \tag{2}$$

$$N = 1/n_l$$

The relative permeability of gas and oil was adjusted using a formula proposed by Coats to interpolate between miscible and immiscible conditions.

$$K_{RG} = F_K * K_{rg}^{imm} + (1 - F_K) * K_{rg}^{mis} \tag{3}$$

$$K_{RO} = F_K * K_{ro}^{imm} + (1 - F_K) * K_{ro}^{mis} \tag{4}$$

In the equations mentioned above, σ_0 signifies the IFT at MMP, and σ represents the IFT at corresponding pressure. The exponent is indicated as n_l . K_{RG} , K_{rg}^{mis} , and K_{rg}^{imm} stand for the gas's modified, miscible, and immiscible relative permeability, respectively. Similarly, the oil's modified, miscible, and immiscible relative permeability are represented by K_{RO} , K_{ro}^{mis} , and K_{ro}^{imm} , respectively.

The residual oil saturation and irreducible gas saturation need to be adjusted:

$$S_{gi} = F_K * S_{gi}^{imm} \tag{5}$$

$$S_{or} = F_K * S_{or}^{imm} \tag{6}$$

$$S_{gn} = \frac{S_g - S_{gi}}{1 - S_{gi} - S_{or}} \tag{7}$$

In this study, the Corey–Brooks (1965) correlation was employed to determine the relative permeability of oil and gas in the immiscible situations:

$$K_{rg}^{imm} = K_{rg} * S_{gn}^{ng} \tag{8}$$

$$K_{ro}^{imm} = K_{ro} * (1 - S_{gn})^{no} \tag{9}$$

$$K_{rg}^{mis} = S_{gn}^{nm} \tag{10}$$

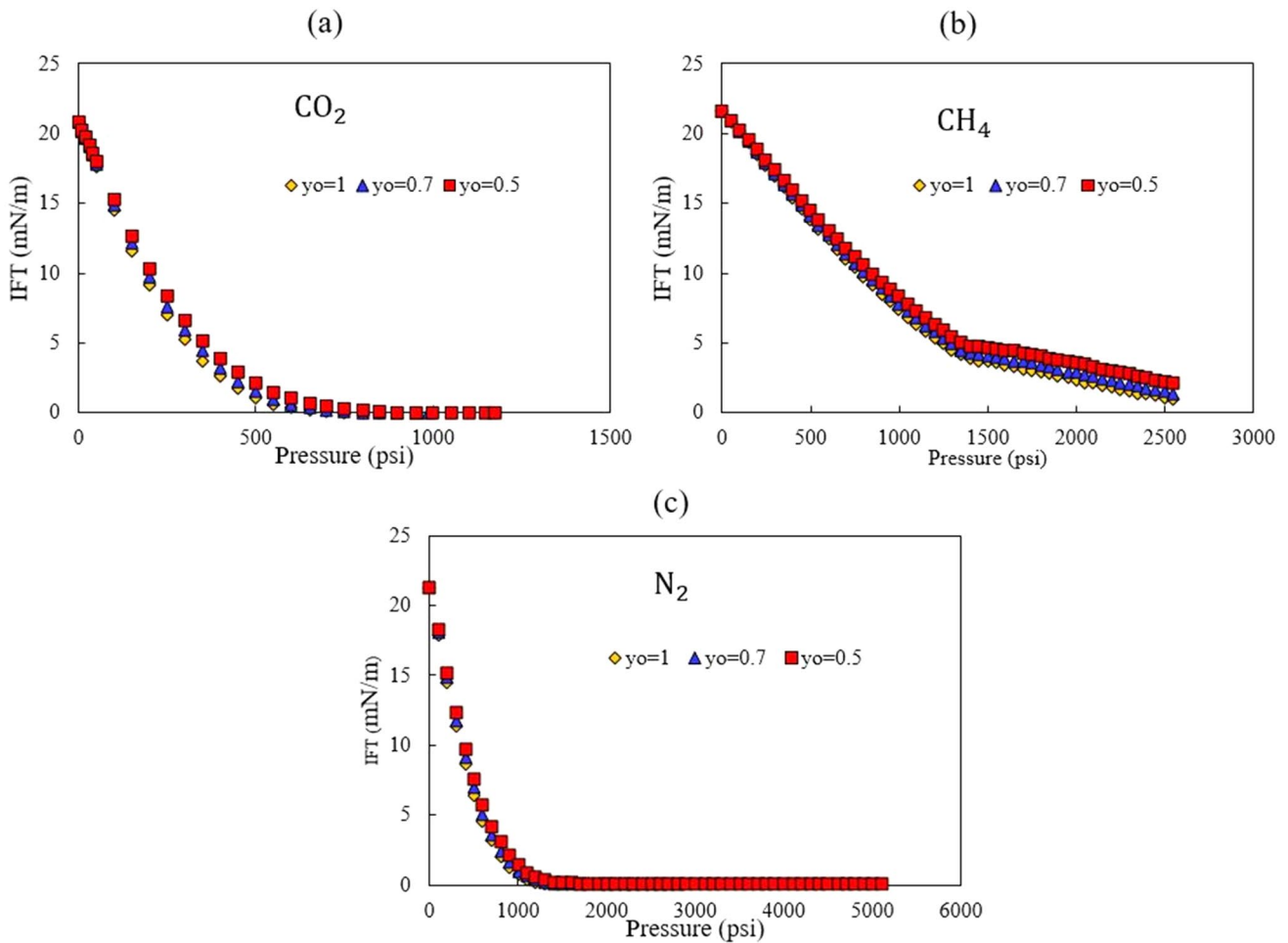


Fig. 4 Effect of mole fraction of oil in the gas phase on the IFT for CO₂, CH₄, and N₂ and live oil system

$$K_{ro}^{mis} = (1 - S_{gn})^{n_m} \tag{11}$$

In the above equations, the modified irreducible gas saturation and residual oil saturation are denoted by S_{gi} and S_{or} , respectively. The residual oil saturation at immiscible conditions is represented as S_{or}^{imm} and S_{gi}^{imm} signifies the irreducible gas saturation in immiscible conditions. The relative permeability of the gas phase at residual oil saturation and the relative permeability of oil at irreducible gas saturation are indicated by K_{rg} and K_{ro} , respectively. In Eqs. (8)–(11) three relative permeability indexes, n_m , n_g , and n_o are introduced. The immiscible relative permeability curve was utilized to determine n_g and n_o , with a value of 1.1 chosen for n_m in this study.

Calculation of viscosity of gas and oil

Viscosity is a crucial parameter in the gas injection. To accurately simulate gas injection, adjusting the viscosity

of both the reservoir and injection fluids is essential. The Todd and Longstaff (1972) model determine the effective viscosity of oil and gas:

$$\mu_{geff} = \mu_g^{1-\omega} * \mu_m^\omega \tag{12}$$

$$\mu_{oeff} = \mu_o^{1-\omega} * \mu_m^\omega \tag{13}$$

$$\left(\frac{1}{\mu_m}\right)^{\frac{1}{4}} = \frac{S'_g}{S'_n} \left(\frac{1}{\mu_g}\right)^{\frac{1}{4}} + \frac{S'_o}{S'_n} \left(\frac{1}{\mu_o}\right)^{\frac{1}{4}} \tag{14}$$

$$S'_g = S_g - S_{gi} \tag{15}$$

$$S'_o = S_o - S_{or} \tag{16}$$

$$S'_n = S'_o - S'_g \tag{17}$$

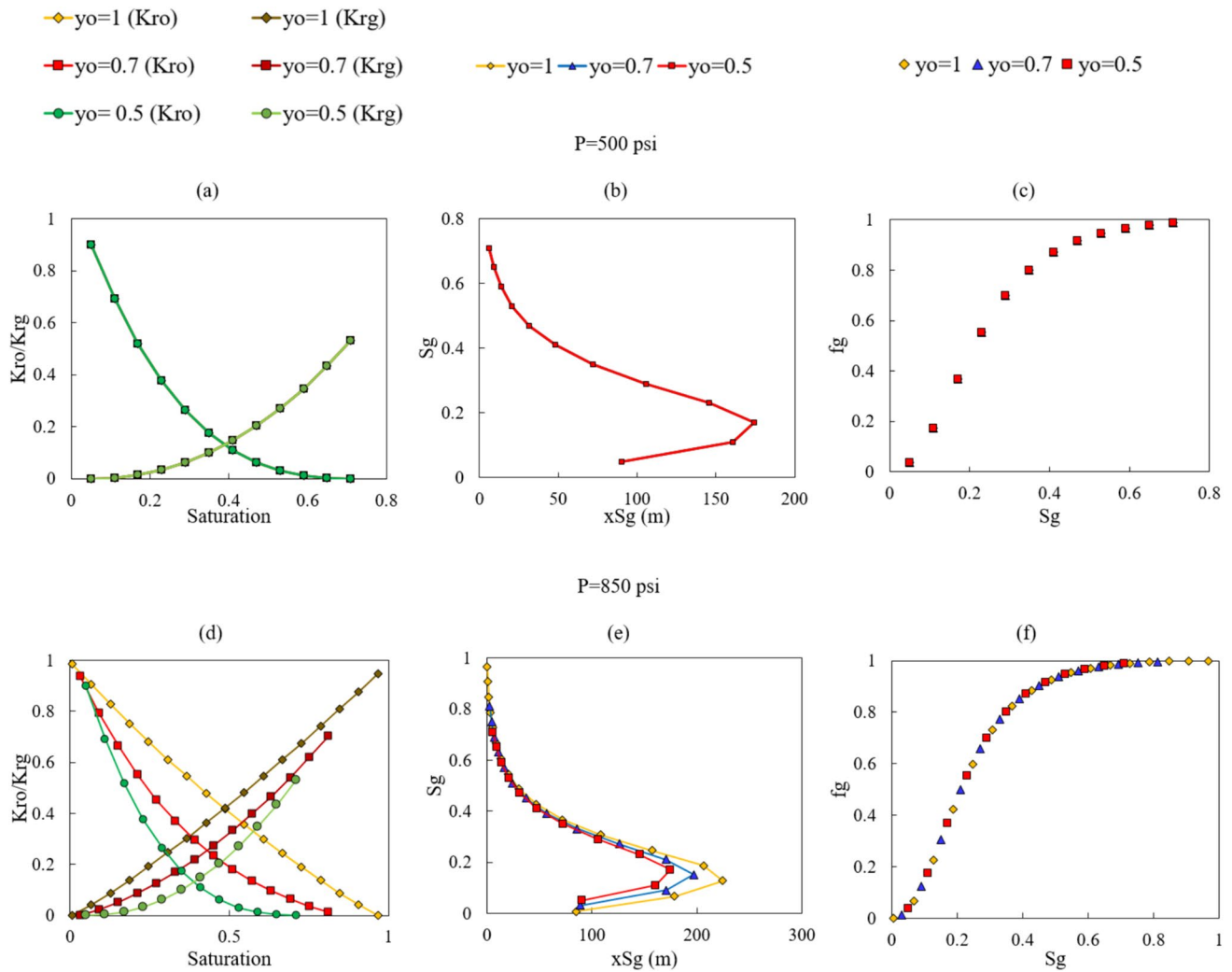


Fig. 5 Effect of mole fraction of oil in the gas phase on the relative permeability, saturation profile, fractional flow curves at an injection pressure of 500 psi and 850 psi for CO₂-live oil system and IFT₀=0.05 mN/m

The viscosity mixing factor, represented by ω , has a value of 1/3 for simulation in the current study.

$$\frac{df_g}{dS_g} = \frac{2V(S_g - 1)S_g}{(V(S_g - 1)^2 + S_g^2)^2} \tag{19}$$

Calculation gas saturation and fractional flow of gas phase

The Buckley–Leverett method is a technique commonly employed to determine the saturation profile and fractional flow in porous media.

$$PVI = \frac{q_i t}{L\phi Area} \tag{20}$$

$$f_g = \frac{S_g^2}{S_g^2 + (1 - S_g)^2 V} \tag{18}$$

$$x_{S_g} = PVI * L \left(\frac{df_g}{dS_g} \right)_{S_g} \tag{21}$$

The study employed various parameters including f_g (fractional flow for the gas phase), $\frac{df_g}{dS_g}$ (derivative of fractional flow of the gas phase with respect to gas saturation), A_{rea} , t (time), L (length), V (volume), ϕ (porosity), PVI

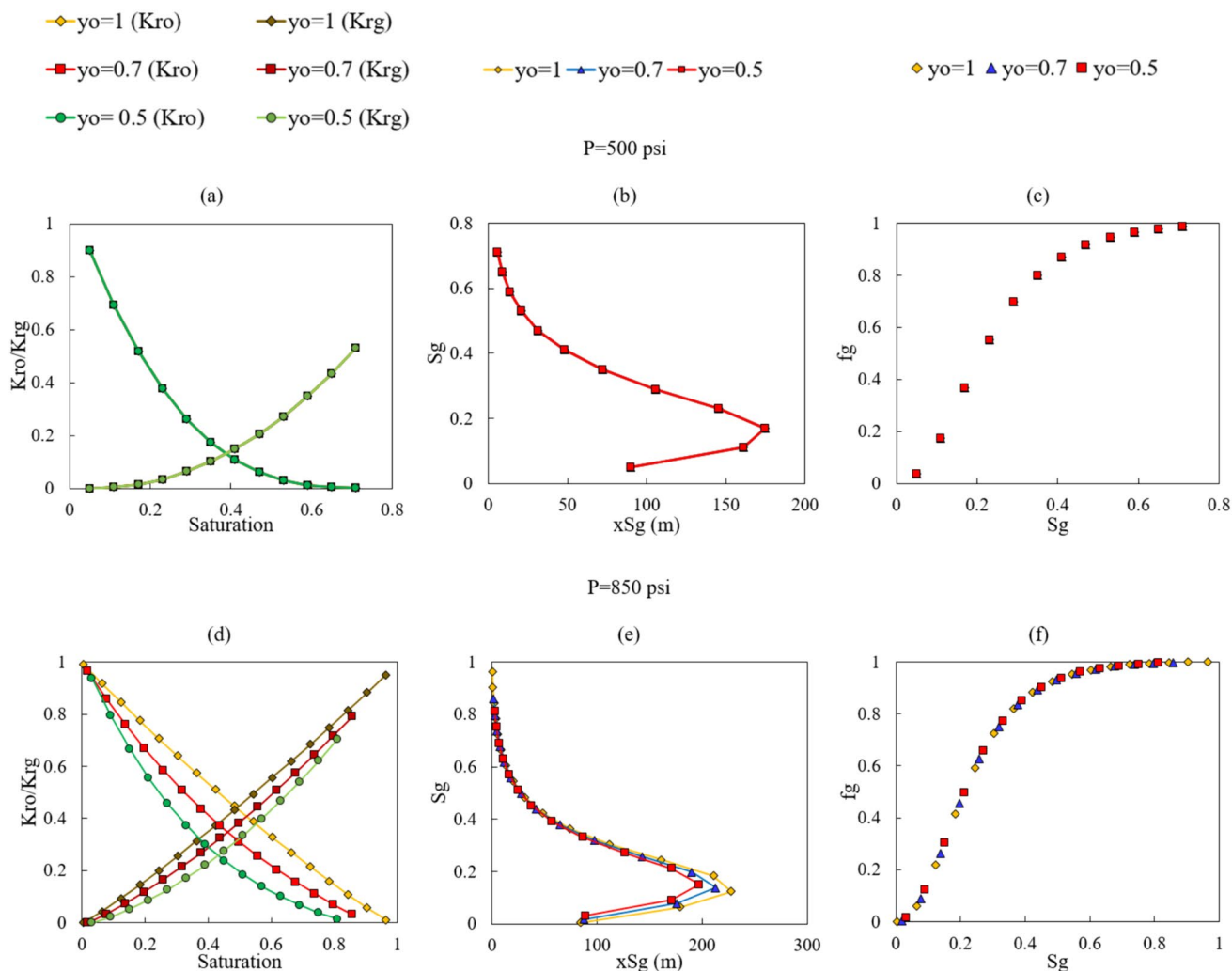


Fig. 6 Effect of mole fraction of oil in the gas phase on the relative permeability, saturation profile, and fractional flow curves at an injection pressure of 500 and 850 psi for CO₂-live oil system and IFT₀=0.5 mN/m

(dimensionless pore volume), q_t (total injection rate), and x_{S_g} (distance traveled by a specific S_g contour) (Dandekar 2013).

Results and discussion

In this section, after presenting the validation of the developed code, the effect of vaporized oil in the gas phase on the IFT of three investigated gas-oil systems (N₂, CO₂, and methane (CH₄)) has been explored. Following that, the impacts of injection pressure, initial IFT₀, and vaporized oil in the gas phase on the gas injection process have been studied. A sensitivity analysis was conducted to investigate how these parameters affect IFT, relative permeability curve, fractional flow, and saturation profile. It is important

to note that this paper examines two types of oil: movable and residual. The results for movable oil are presented in subsequent sections, while those for residual oil are available in the supplementary file.

Numerical simulation

Table 1 illustrates the values for every input parameter:

To assess the developed model, experimental data was used for validation. The oil density, solution gas-oil ratio, and oil formation volume factor are the key parameters needed to calculate the IFT of the system. The validation of these parameters was carried out for the developed model. As depicted in Fig. 2, the model can precisely predict these parameters with minimal error. Moreover, the relative permeability of oil and gas under immiscible

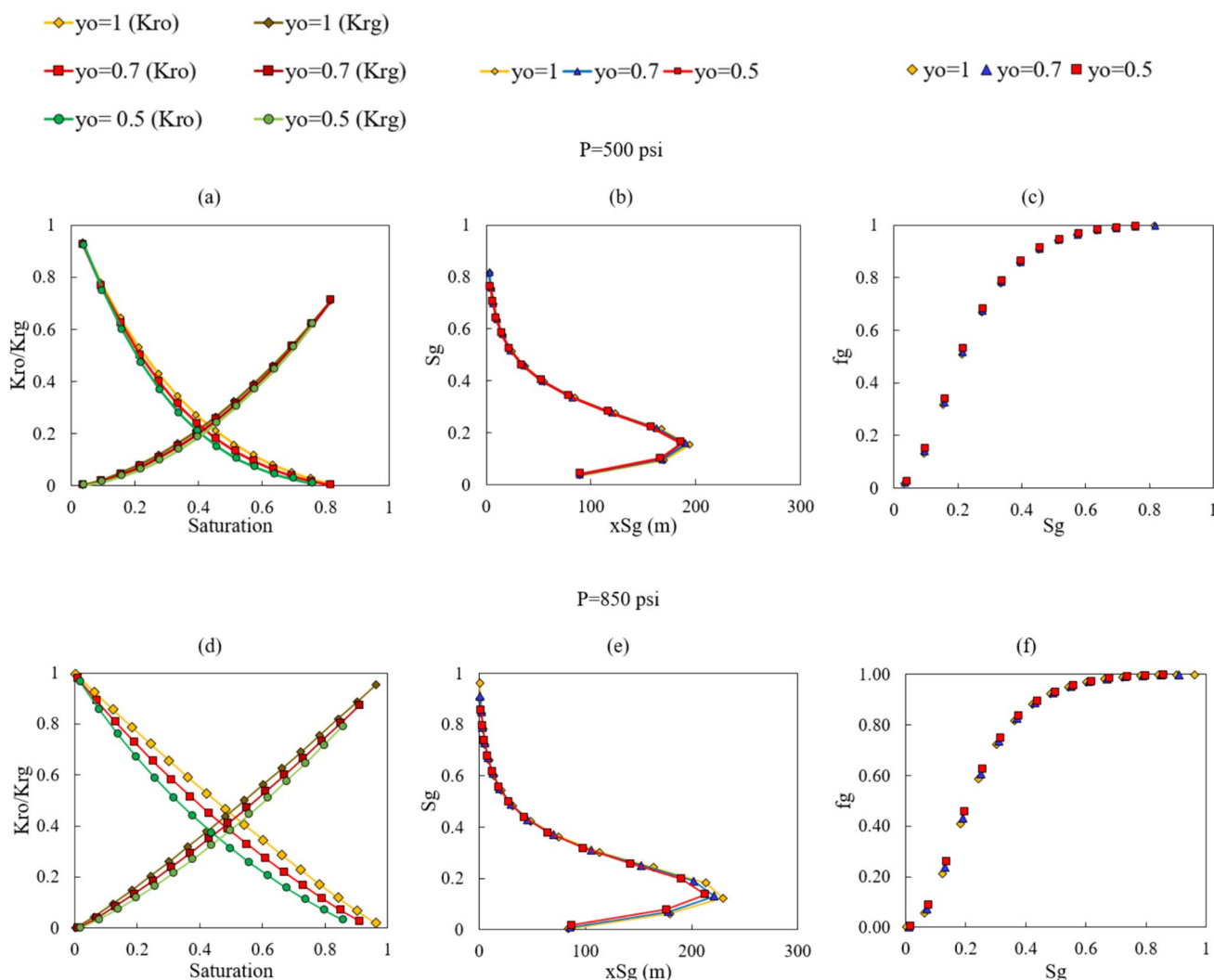


Fig. 7 Effect of mole fraction of oil in the gas phase on the relative permeability, saturation profile, and fractional flow curves at an injection pressure of 500 and 850 psi for CO₂-live oil system and IFT₀=5 mN/m

conditions is another vital parameter in the developed model. Figure 2 presents a comparison between the predictions of the relative permeability-based developed model and the experimental data, demonstrating satisfactory accuracy in relative permeability prediction.

The last stages of assessing the developed model involves forecasting the fractional flow curve. By leveraging the simulation findings from Mu et al. (2019), the model's accuracy in predicting the fractional flow curve has been evaluated. Based on Fig. 3, developed model in the present study produces satisfactory results, aligning well with the fractional flow predictions from Mu et al. (2019).

Effect of vaporized oil in the gas phase for live oil

As previously mentioned, the black oil model generally assumes that $r_v = 0$ resulting in $y_o = 1$, and $y_g = 0$. A sensitivity analysis was conducted on the y_o and y_g values in this section. Three distinct scenarios were investigated: $y_o = 1$ and $y_g = 0$, $y_o = 0.7$ and $y_g = 0.3$, and $y_o = 0.5$ and $y_g = 0.5$. Figure 4 shows the influence of y_o and y_g on the IFT for each gas.

As shown in Fig. 4, the variation in y_o had an impact on both the IFT curve and the near-miscible pressure. In this study, the near-miscible pressure was defined as the pressure at which the IFT reached a value of 1 mN/m. For CO₂, the near-miscible pressure values were 505, 548, 602

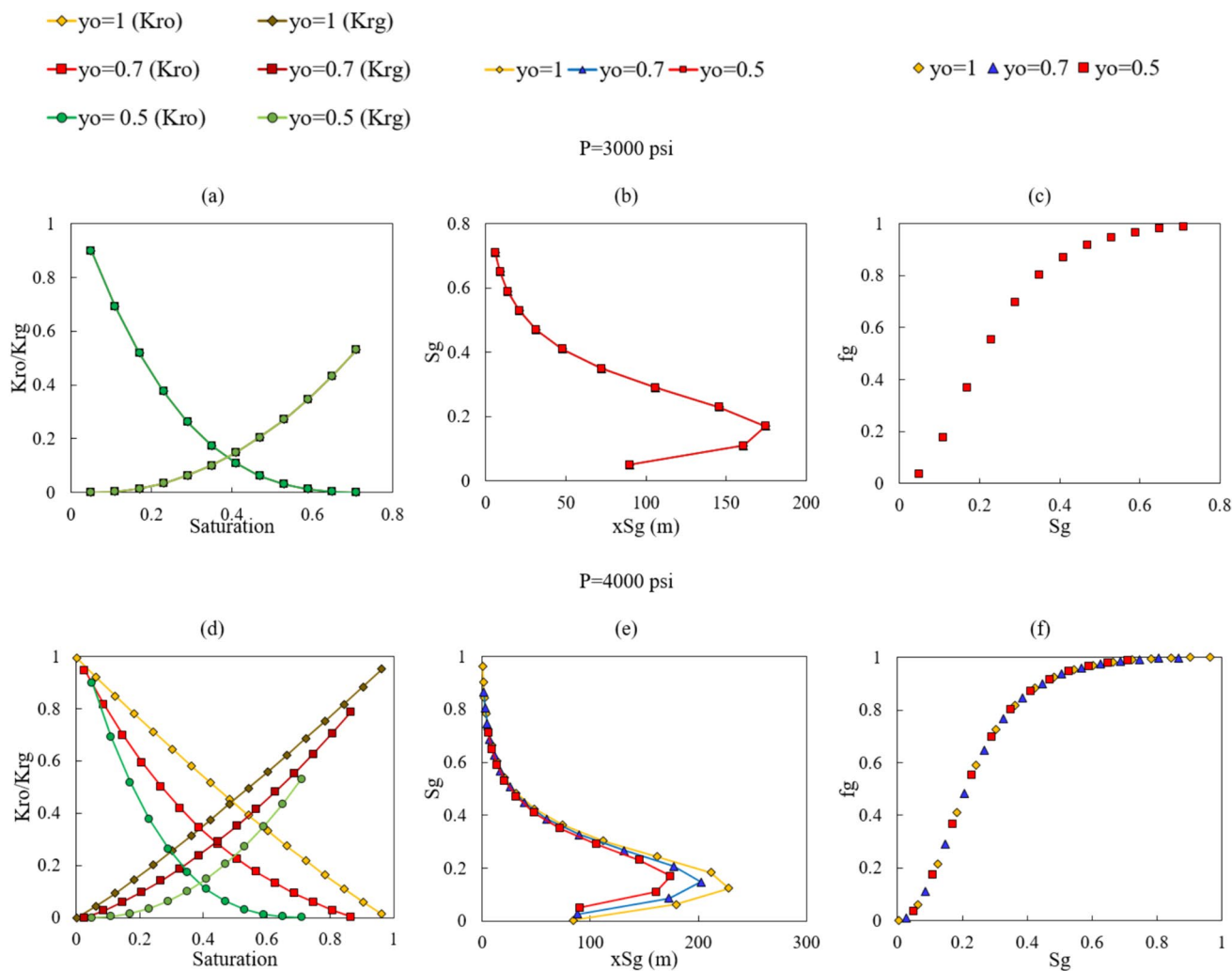


Fig. 8 Effect of mole fraction of oil in the gas phase on the relative permeability curve, saturation profile, and fractional flow curve at an injection pressure of 3000 psi and 4000 psi for CH₄-live oil system and IFT₀=0.05 mN/m

psi at $y_o = 1$, $y_o = 0.7$, and $y_o = 0.5$, respectively (Subplot (a) of Fig. 4). In Fig. 4, Subplot (b) illustrates that the near-miscible pressure of CH₄ at $y_o = 1$, $y_o = 0.7$, $y_o = 0.5$ were 2500, 2700, and 3050 psi, respectively. The near-miscible pressure values for N₂ at $y_o = 1$, $y_o = 0.7$, and $y_o = 0.5$ were 934 psi, 994 psi, and 1072 psi, respectively (Subplot (c) of Fig. 4). Reducing y_o led to an increase in near-miscible pressure, while increasing y_o resulted in a decrease in the IFT of the system (Fig. 4). In other words, the condensing mechanism produced lower IFT and near-miscible pressure, whereas shifting to condensing-vaporizing mechanism increased both. These trends were consistent across all three gases. Notably, the impact of the mechanism on the CH₄-live oil system was more significant compared to the other gases, indicating a stronger effect on the hydrocarbon gas than on N₂ and CO₂.

Effect of vaporized oil in the gas phase on live oil-gas system

In this section, the impact of vaporized oil in the gas phase on a live oil-gas system was examined. Figure 5 shows the relative permeability curve, saturation profile, and fractional flow curve for the CO₂-live oil system at IFT₀ of 0.05 mN/m, under two different injection pressure: 500 (Subplots (a)–(c)) and 850 psi (Subplots (d)–(f)).

Based on Subplots (a)–(c) of Fig. 5, at a low injection pressure of 500 psi, the effect of y_o is minimal. However, increasing the injection pressure to 850 psi revealed its impact on y_o . Changing in y_o led to alterations in the relative permeability, saturation profile, and fractional flow, as observed in Subplots (d)–(f) of Fig. 5. The saturation profile presented in this paper is theoretically correct but

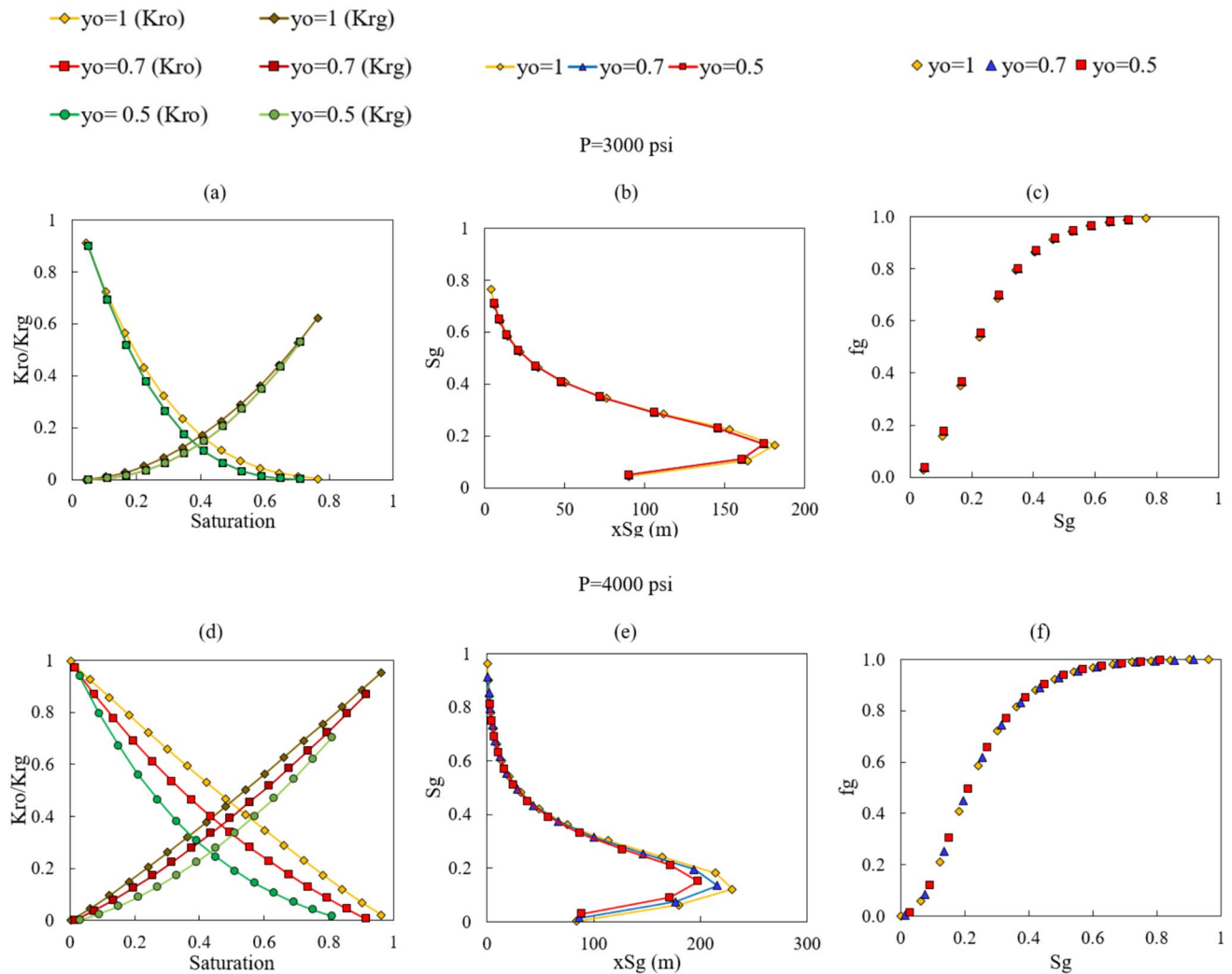


Fig. 9 Effect of mole fraction of oil in the gas phase on the relative permeability curve, saturation profile, and fractional flow curve at an injection pressure of 3000 psi and 4000 psi for CH_4 -live oil system and $\text{IFT}_0=0.5$ mN/m

unattainable in practice. While adjustments have been proposed in the literature, we maintained the original saturation profile in our study. Shifting from condensing to condensing-vaporizing at higher pressure resulted in a decrease in fluids' relative permeability. This shift is evident in the gas saturation profile (Subplots (e) and (f) of Fig. 5), showing faster gas movement in the domain and higher gas fractional flow when the condensing mechanism dominates.

As the $\text{IFT}_0=0.05$, at a higher injection pressure, the impact of y_o was observed for $\text{IFT}_0=0.5$, as shown in Fig. 6.

Similar to the previous results, the condensing mechanism led to higher gas relative permeability, faster gas movement, and a higher f_g .

When $\text{IFT}_0=5$, the y_o factor influences the model output at both injection pressures, as shown in Fig. 7, unlike the cases where IFT_0 was 0.05 and 0.5.

Methane is another gas used as an injection fluid. Figures 8, 9, 10 show the results of injecting methane into live oil. As indicated by them, the impact of y_o on the model output is significantly stronger at high injection pressure than at low pressure.

At all pressures and IFT_0 values, with the exception of 3000 psi when IFT_0 is 0.05, the effect of the condensation mechanism results in decreased the fluids' relative permeability, accelerated gas displacement within the domain, and higher f_g (Figs. 8, 9, 10).

In the last scenario, nitrogen was introduced into live oil under two injection pressures of 1000 psi and 2000 psi. Figures 11, 12 and 13 display the impact of y_o during nitrogen injection.

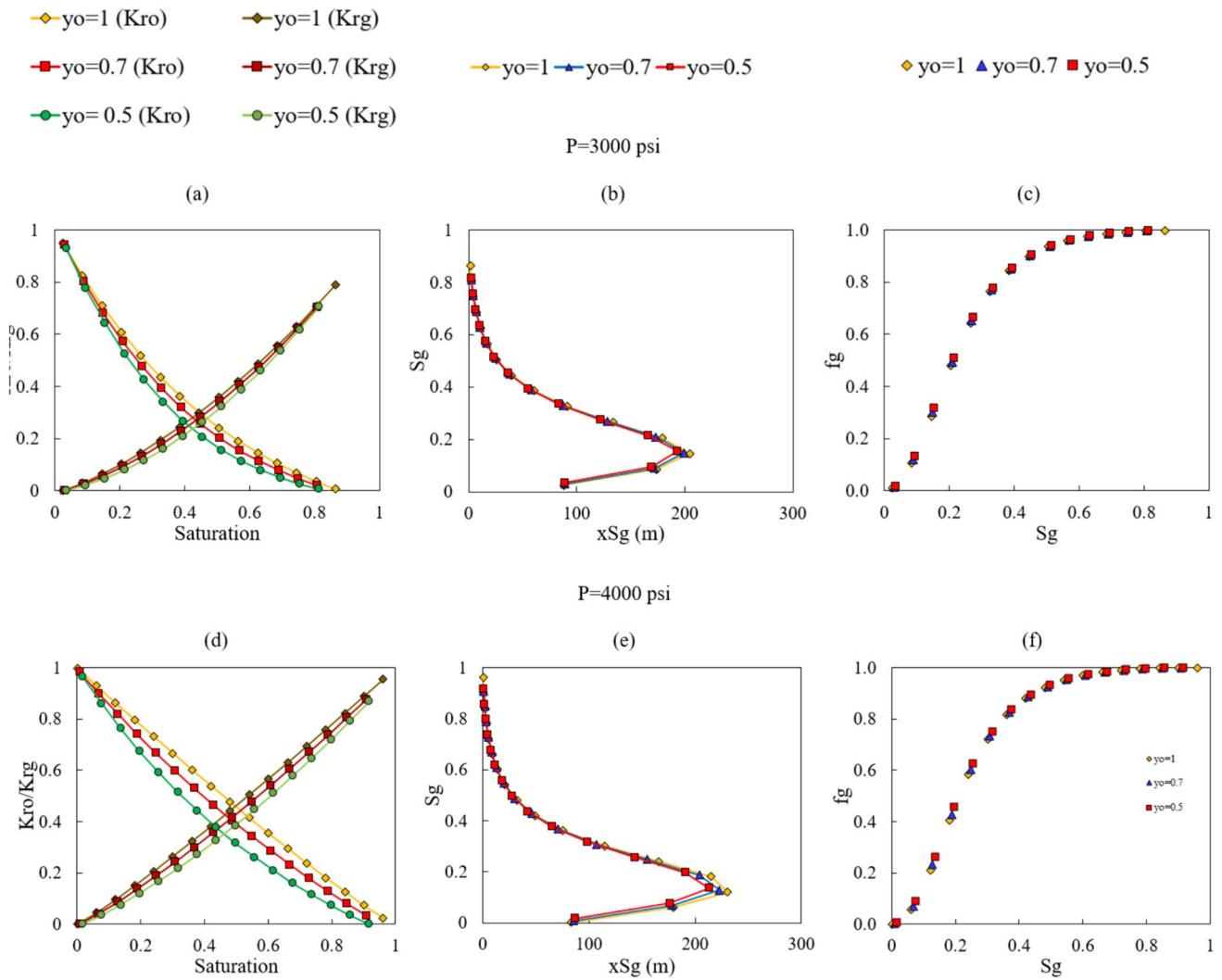


Fig. 10 Effect of mole fraction of oil in the gas phase on the relative permeability curve, saturation profile, and fractional flow curve at an injection pressure of 3000 psi and 4000 psi for CH₄-live oil system and IFT0 = 5 mN/m

As depicted in Subplots (a)–(f) of Figs. 11, 12 and 13, the impact of y_o is minor at low injection pressures of 1000 psi. However, as the injection pressure rises, the significance of y_o increases. This implies that utilization of nitrogen as an injection gas has a greater effect on the model's output.

Effect of injection pressure on the output of the model for live oil

Injection pressure plays a crucial role in influencing the relative permeability curve, saturation profile, and fractional flow curve. The impact of injection pressure on the

performance of individual gases was assessed, assuming an IFT0 of 0.5 and dominance of the condensing mechanism in the system. In Figs. 14, 15 and 16, it is evident that as the injection pressure rises, the relative permeability of fluids increases. Moreover, higher injection pressure accelerates gas movement within the domain, resulting in an elevated gas fractional flow rate.

Effect of IFT0 on the output of the model for live oil

The impact of IFT0 on the model's output was examined as the final sensitivity analysis in this study. Higher injection and condensing mechanisms were found to have a greater

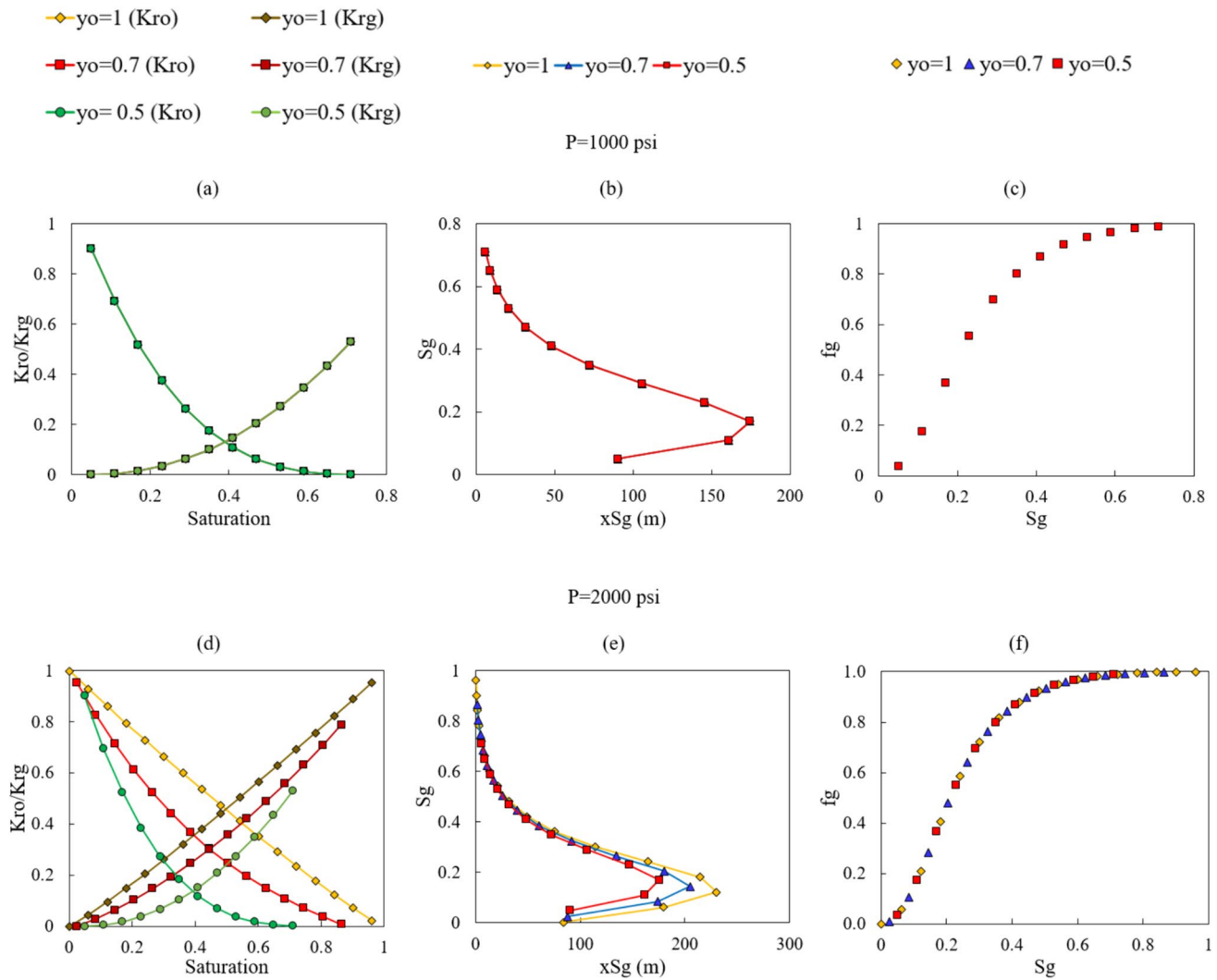


Fig. 11 Effect of mole fraction of oil in the gas phase on the relative permeability curve, saturation profile, and fractional flow curve at an injection pressure of 1000 psi and 2000 psi for N_2 -live oil system and $IFT_0 = 0.05$ mN/m

impact on the model's output. Thus, the sensitivity analysis of IFT_0 was carried out with an emphasis on the condensing mechanism and higher injection pressure for each gas. The influence of IFT_0 on the output was found to be comparable to that of injection pressure on the model's output (Figs. 17, 18 and 19). With an increase in IFT_0 , the relative permeability of fluids was observed to increase (Subplot (a) of Figs. 17, 18 and 19). Moreover, an increase in IFT_0 led to faster gas movement within the domain (Subplot (b) of Figs. 17, 18 and 19). The impact of IFT_0 on the fractional flow curve is highlighted in Subplot (c) of Figs. 17, 18 and 19, showcasing a noticeable effect.

In summary, when the condensing mechanism is the dominant mechanism in the gas injection process, a lower IFT and near-miscible pressure are achieved (Fig. 4). In other words, the condensing mechanism leads to a lower IFT and the earlier generation of the miscibility condition, which can result in better efficiency for the gas injection process. This is reflected in the model's output, where governing the condensing mechanism in the IFT measurement results in a more rapid flow of gas through the medium and an increase in the relative permeability curve of fluids (Figs. 5, 6, 7, 8, 9, 10, 11, 12 and 13). Furthermore, in the condensing mechanism and $IFT_0 = 0.5$, a higher injection

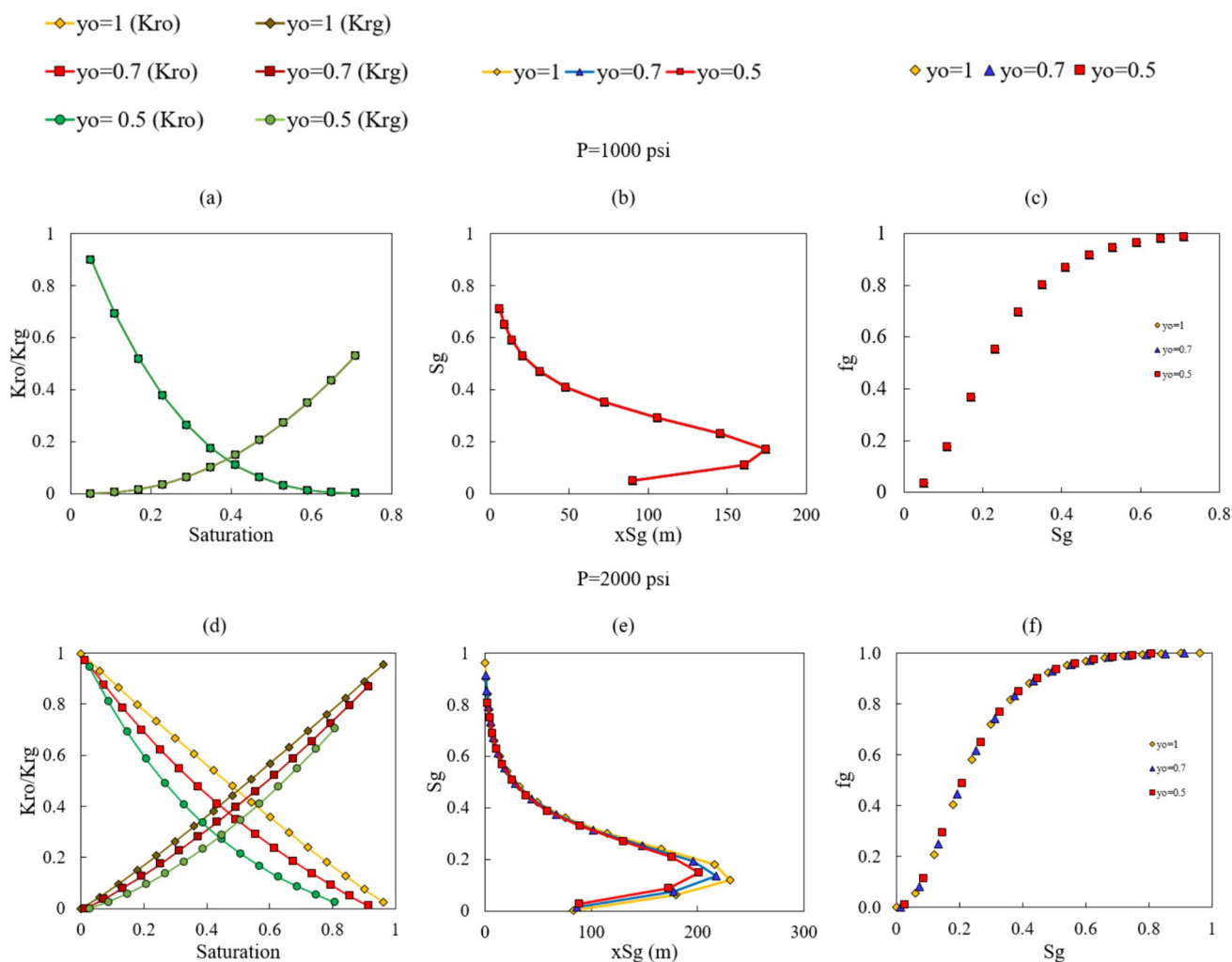


Fig. 12 Effect of mole fraction of oil in the gas phase on the relative permeability curve, saturation profile, and fractional flow curve at an injection pressure of 1000 psi and 2000 psi for N_2 -live oil system and $IFT_0=0.5$ mN/m

pressure resulted in a faster movement of fluid and an increase in the relative permeability of fluids (Figs. 14, 15, and 16). This behavior has been observed in the sensitivity analysis of IFT_0 , where a higher IFT_0 resulted in an increase in the relative permeability of fluids and a faster movement of gas in the medium (Figs. 17, 18 and 19). It is worth mentioning that, similar to the effect of vaporized oil in the gas phase, there is no specific trend for the fractional flow curve with changes in injection pressure and IFT_0 . Therefore, three factors, including the condensing mechanism, higher injection pressure, and higher IFT_0 , result in better efficiency during the gas injection process as follows:

1. When the condensing mechanism is dominant in the medium, the injection fluid displaces the medium's fluid in a piston-like manner. This behavior is clearly evident

in the relative permeability curve, where fluids have greater relative permeability during this mechanism.

2. Higher injection pressure during gas injection, while the condensing mechanism is dominant, results in more forces to push reservoir fluid. The higher relative permeability of the fluid and faster movement of gas are indications of the effect of injection pressure.
3. By increasing the IFT_0 , the miscibility condition occurs sooner, resulting in increased efficiency of the gas injection process.

It is noteworthy that all above-mentioned behaviors also holds true for a dead oil–gas system.

In the current study, the impact of gas injection is being explored. The developed code allows for the analysis of gas injection effectiveness in different conditions, including immiscible, miscible, and near-miscible states by

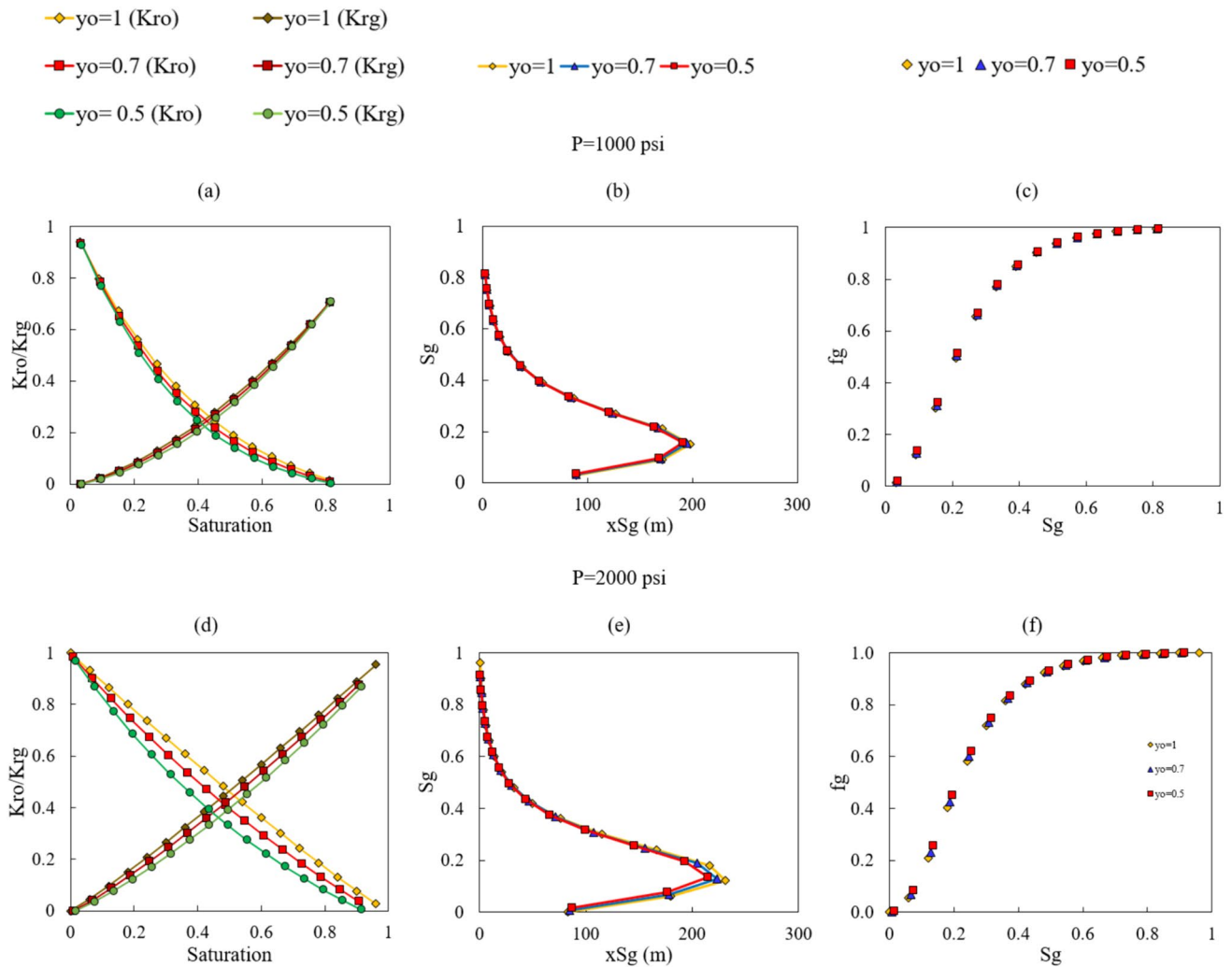


Fig. 13 Effect of mole fraction of oil in the gas phase on the relative permeability curve, saturation profile, and fractional flow curve at an injection pressure of 1000 psi and 2000 psi for N_2 -live oil system and $IFT_0=5$ mN/m

adjusting fluid permeability and viscosity. This developed code enables a comprehensive evaluation of injection gas performance before implementing EOR techniques in the reservoir. By assessing different injection gases under varied conditions, investigating the effects of various mechanisms, injection pressure, and IFT_0 , informed decisions can be made when selecting an EOR method. It is crucial to thoroughly review and analyze variations in injection and reservoir fluid compositions to accurately simulate gas injection processes. Nevertheless, it should be noted that the developed code does not support investigating or determining the gas injection mechanism.

Conclusions

1. For both live and dead oil, the condensing mechanism resulted in decreased interfacial tension (IFT) and near-miscible pressure, while switching to a condensing-vaporizing mechanism led to an increase in both.
2. The impact of the mechanism on the methane-oil system was more significant compared to the other gases, indicating a stronger effect on the hydrocarbon gas than on nitrogen and carbon dioxide.
3. Control over the condensing mechanism during the IFT measurement leads to enhanced gas flow rate within the

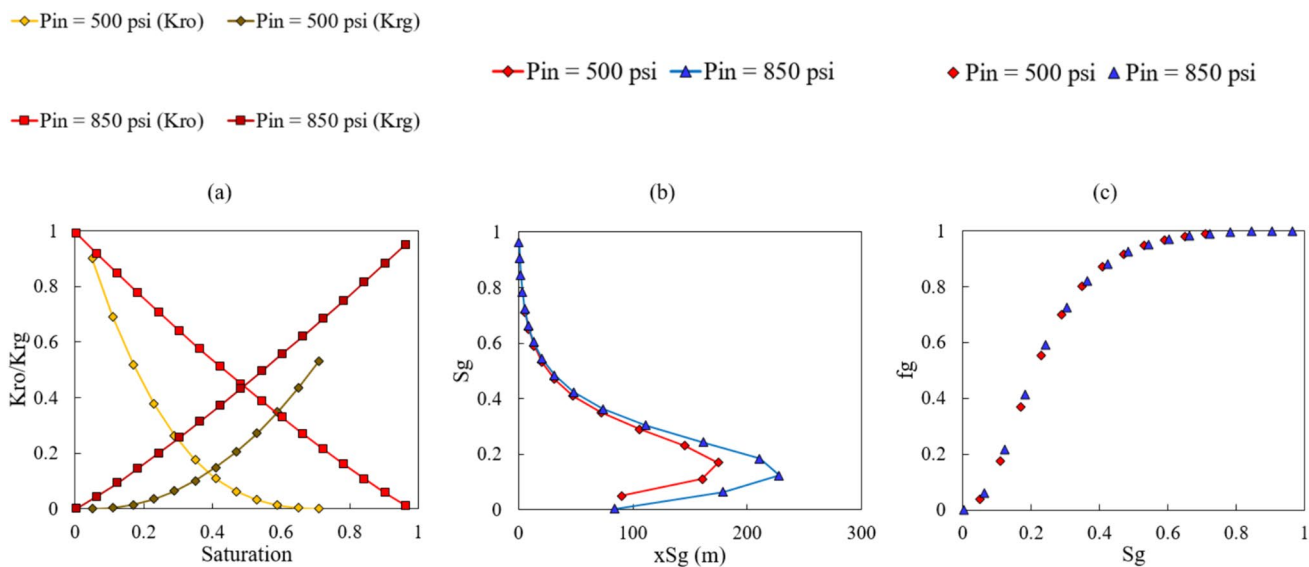


Fig. 14 Effect of injection pressure for CO₂ injection on the **a** relative permeability, **b** saturation profile, **c** fractional flow curve of live oil at IFT₀=0.5 and y_o=1

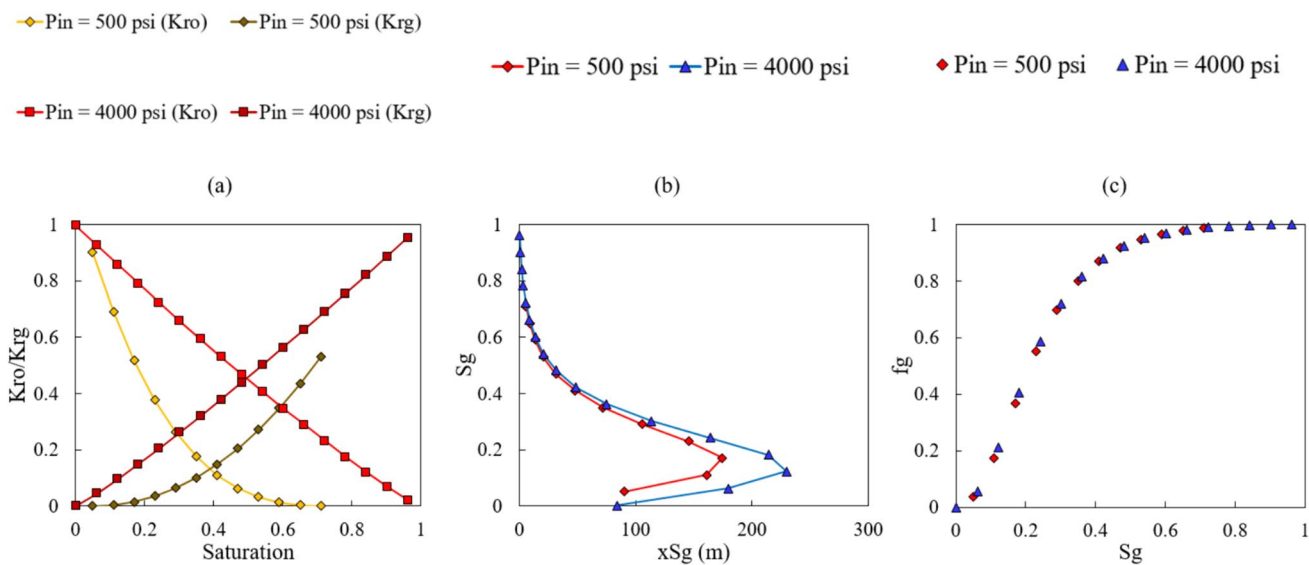


Fig. 15 Effect of injection pressure for CH₄ injection on the **a** relative permeability, **b** saturation profile, **c** fractional flow curve of live oil at IFT₀=0.5 and y_o=1

- medium, along with an elevation in fluids' relative permeability curve.
- In the condensing mechanism and interfacial tension at the minimum miscible pressure (IFT₀) equal to 0.5, a higher injection pressure led to a faster fluid movement and an improved relative permeability of fluids.

- Higher IFT₀ led to an increase in the relative permeability of fluids and a faster gas movement in the medium.
- The impact of IFT₀ on the dead oil–gas system was higher than on the live oil–gas system.

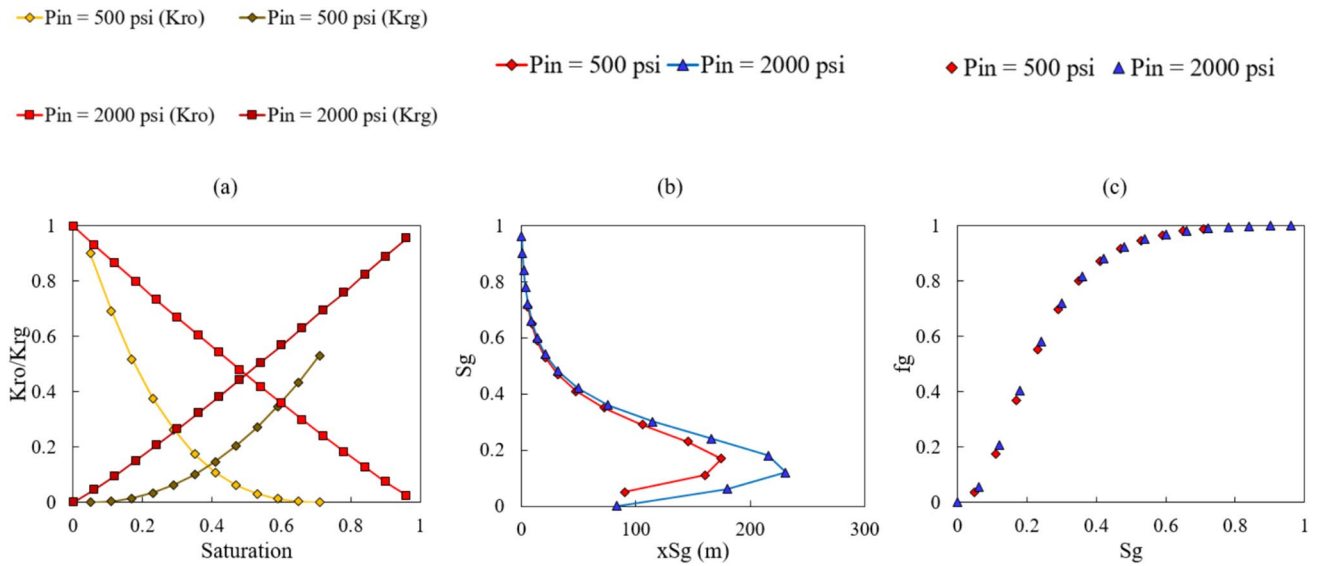


Fig. 16 Effect of injection pressure for N_2 injection on the **a** relative permeability, **b** saturation profile, **c** fractional flow curve of live oil at $IFT_0=0.5$ and $y_o=1$

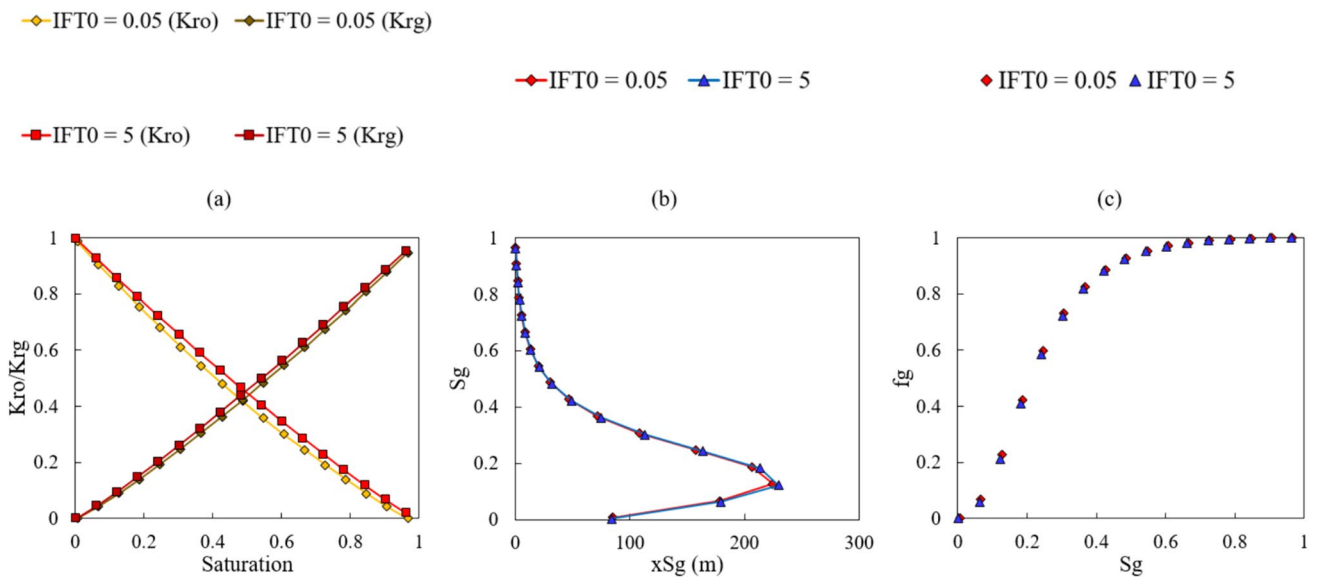


Fig. 17 Effect of IFT_0 for CO_2 injection on the **a** relative permeability, **b** saturation profile, **c** fractional flow curve of live oil at 850 psi and $y_o=1$

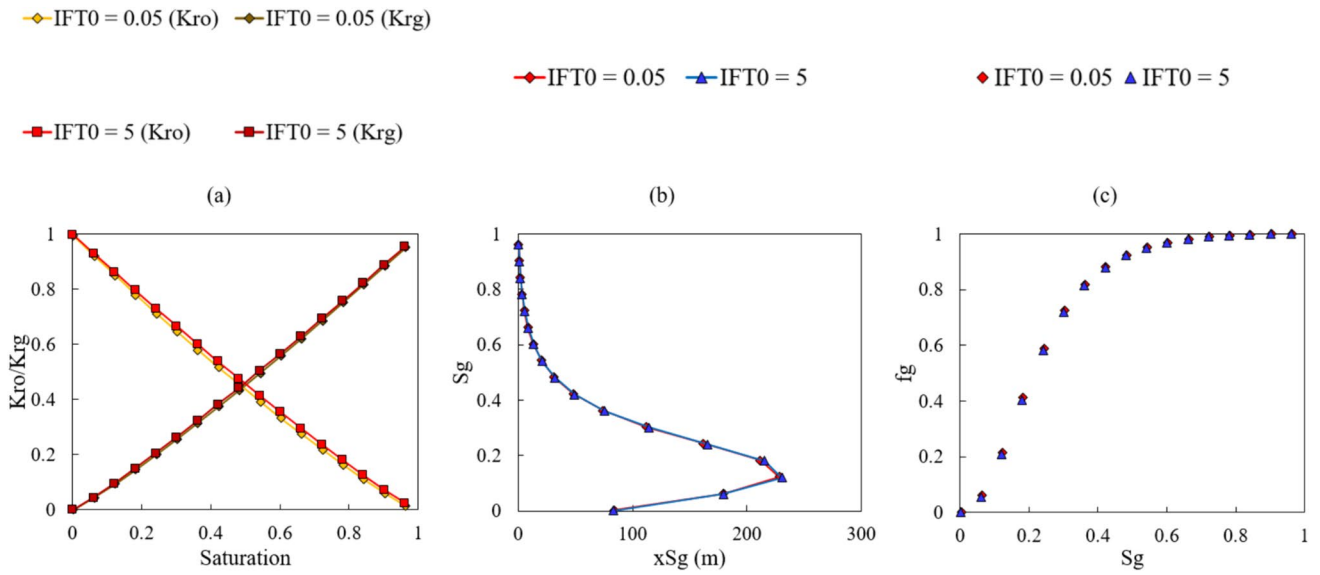


Fig. 18 Effect of IFT0 for CH₄ injection on the **a** relative permeability, **b** saturation profile, **c** fractional flow curve of live oil at 4000 psi and yo=1

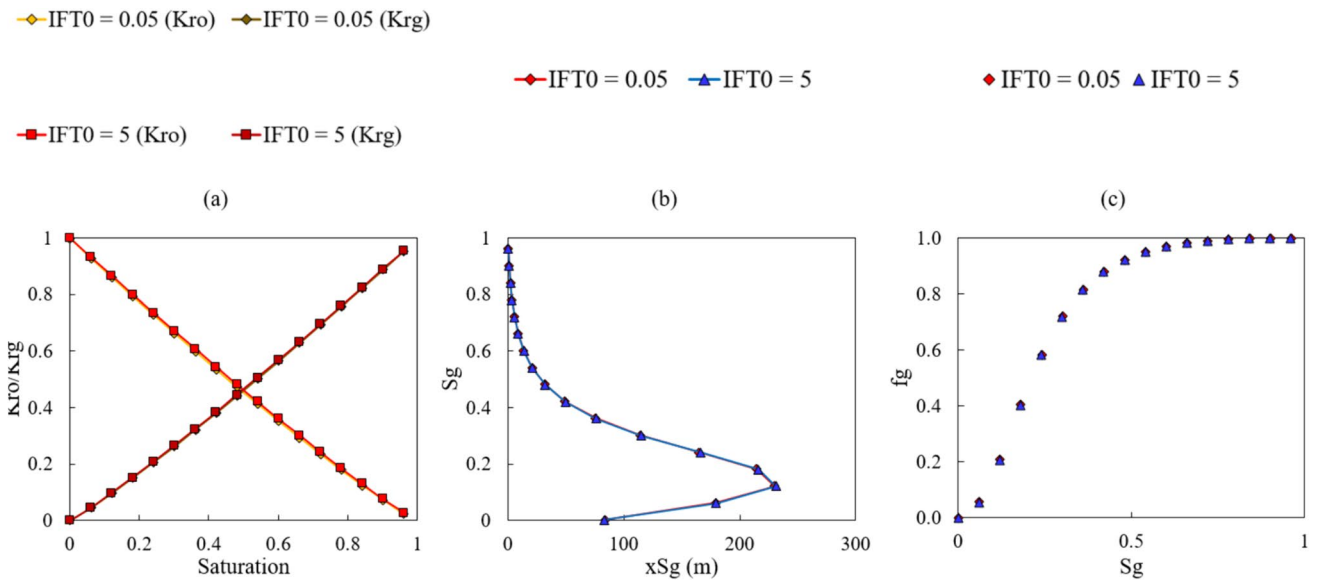


Fig. 19 Effect of IFT0 for N₂ injection on the **a** relative permeability, **b** saturation profile, **c** fractional flow curve of live oil at 2000 psi and yo=1

Appendix

The parameters used in the Ramey correlation can be calculated by Eqs. (22)–(34) (Ramey Jr 1973):

$$M_g = 28.97 * \gamma_g \tag{22}$$

$$P_g = 25.2 + 2.86M_g \tag{23}$$

$$M_o = 6084 / (\gamma_{API} - 5.9) \tag{24}$$

$$P_o = (2.376 + 0.0102\gamma_{API})M_o \tag{25}$$

$$y_o = \left[1 + \frac{7.521 * 10^{-6} M_o}{\gamma_o r_v} \right]^{-1} \quad (26) \quad Z = A + \frac{1-A}{e^B} + CP_{pr}^D \quad (39)$$

$$y_g = 1 - y_o \quad (27) \quad A = 1.39(T_{pr} - 0.92)^{0.5} - 0.36T_{pr} - 0.10 \quad (40)$$

$$x_o = \left[1 + \frac{7.521 * 10^{-6} R_s M_o}{\gamma_o} \right]^{-1} \quad (28) \quad B = (0.62 - 0.23T_{pr})P_{pr} + \left(\frac{0.066}{T_{pr} - 0.86} - 0.037 \right) P_{pr}^2 + \frac{0.32P_{pr}^2}{10^E} \quad (41)$$

$$x_g = 1 - x_o \quad (30) \quad C = 0.132 - 0.32 \log(T_{pr}) \quad (42)$$

$$\rho_g = 9.3184 * 10^{-2} \frac{PM_{go}}{62.4 * ZT} \quad (31) \quad D = 10^F \quad (43)$$

$$\rho_o = \frac{\gamma_o + 2.179 * 10^{-4} \gamma_g R_s}{B_o} \quad (32) \quad E = 9(T_{pr} - 1) \quad (44)$$

$$M_{go} = y_o M_o + y_g M_g \quad (33) \quad F = 0.3106 - 0.49T_{pr} + 0.1824T_{pr}^2 \quad (45)$$

In these equations, M_g , γ_g , and R_s represent the molecular weight of the gas, its specific gravity, and gas-oil ratio, respectively. Compressibility factor, pressure, and temperature are shown by Z , P , and T . The specific gravity of oil is displayed by γ_o , and B_o shows the oil formation volume factor. γ_o and γ_{API} can be relate to each other using the formula: $\gamma_{API} = \frac{141.5}{\gamma_o} - 131.5$. Vaporized oil in the gas phase is represented by r_v . It is important to note that in the black oil model, $r_v = 0$, which implies $y_g = 0$, and $y_o = 1$.

Sutton (1985), Brill and Beggs (1973), Standing's (Standing 1947) correlations can be employed to calculate critical pressure and temperature, compressibility factor, solution gas-oil ratio, and oil formation volume factor. The Eqs. (34)–(48) in the appendix show correlations that were utilized to calculate the above-mentioned parameters.

$$P_{pc} = 756.8 - 131.07 * \gamma_g - 3.6 * \gamma_g^2 \quad (34)$$

$$P_{pr} = \frac{P}{P_{pc}} \quad (35)$$

$$T_{pc} = 169.2 + 349.5 * \gamma_g - 74 * \gamma_g^2 \quad (36)$$

$$T_{pr} = \frac{T}{T_{pc}} \quad (37)$$

$$tpr = \frac{1}{T_{pr}} \quad (38)$$

$$R_s = \gamma_g \left[\left(\frac{P}{18.2} + 1.4 \right) 10^a \right]^{1.2048} \quad (46)$$

$$a = 0.00091(T - 460) - 0.0125\gamma_{API} \quad (47)$$

$$B_o = 0.9759 + 0.000120 \left[R_s \left(\frac{\gamma_g}{\gamma_o} \right)^{0.5} + 1.25(T - 460) \right]^{1.2} \quad (48)$$

Pseudocritical pressure and temperature are shown by P_{pc} and T_{pc} , while pseudoreduced pressure and pseudoreduced temperature are denoted by P_{pr} and T_{pr} , respectively.

Supplementary Information The online version contains supplementary material available at <https://doi.org/10.1007/s13202-024-01821-8>.

Acknowledgements The authors also would like to express their appreciation to Iran's National Elites Foundation for its financial supports.

Funding The authors declare that they have no known competing financial interests or personal relationships that could have appeared to influence the work reported in this paper.

Declarations

Conflict of interest The authors declare no competing interests.

Open Access This article is licensed under a Creative Commons Attribution 4.0 International License, which permits use, sharing, adaptation, distribution and reproduction in any medium or format, as long as you give appropriate credit to the original author(s) and the source, provide a link to the Creative Commons licence, and indicate if changes were made. The images or other third party material in this article are included in the article's Creative Commons licence, unless indicated otherwise in a credit line to the material. If material is not included in the article's Creative Commons licence and your intended use is not permitted by statutory regulation or exceeds the permitted use, you will

need to obtain permission directly from the copyright holder. To view a copy of this licence, visit <http://creativecommons.org/licenses/by/4.0/>.

References

- Ahmadi MA, Mahmoudi B (2016) Development of robust model to estimate gas–oil interfacial tension using least square support vector machine: experimental and modeling study. *J Supercrit Fluids* 107:122–128
- Akutsu T, Yamaji Y, Yamaguchi H, Watanabe M, Smith RL Jr, Inomata H (2007) Interfacial tension between water and high pressure CO₂ in the presence of hydrocarbon surfactants. *Fluid Phase Equilib* 257(2):163–168
- Beggs DH, Brill JP (1973) A study of two-phase flow in inclined pipes. *J Petrol Technol* 25(05):607–617
- Bennion DB, Bachu S (2008) Correlations for the interfacial tension between supercritical phase CO₂ and equilibrium brines at in situ conditions. Paper presented at the SPE annual technical conference and exhibition. <https://doi.org/10.2118/114479-MS>
- Brooks RH (1965) Hydraulic properties of porous media. Colorado State University, New York
- Chen Z, Yang D (2019) Correlations/estimation of equilibrium interfacial tension for methane/CO₂-water/brine systems based on mutual solubility. *Fluid Phase Equilib* 483:197–208
- Chen C, Balhoff M, Mohanty KK (2014) Effect of reservoir heterogeneity on primary recovery and CO₂ huff ‘n’ puff recovery in shale-oil reservoirs. *SPE Reservoir Eval Eng* 17(03):404–413. <https://doi.org/10.2118/164553-PA>
- Chiquet P, Daridon J-L, Broseta D, Thibeau S (2007) CO₂/water interfacial tensions under pressure and temperature conditions of CO₂ geological storage. *Energy Convers Manag* 48(3):736–744
- Chun B-S, Wilkinson GT (1995) Interfacial tension in high-pressure carbon dioxide mixtures. *Ind Eng Chem Res* 34(12):4371–4377
- Coats KH (1980) An equation of state compositional model. *Soc Petrol Eng J* 20(05):363–376
- Da Rocha SR, Harrison KL, Johnston KP (1999) Effect of surfactants on the interfacial tension and emulsion formation between water and carbon dioxide. *Langmuir* 15(2):419–428
- Dalvand K, Heydarian A (2015) Determination of gas-oil interfacial tension. *Energy Sources Part A Recov Utilizat Environ Effects* 37(16):1790–1796
- Dandekar AY (2013) Petroleum reservoir rock and fluid properties. CRC Press, London
- Escrochi M, Mehranbod N, Ayatollahi S (2013) The gas–oil interfacial behavior during gas injection into an asphaltenic oil reservoir. *J Chem Eng Data* 58(9):2513–2526
- Fatemi SM, Sohrabi M (2013) Experimental investigation of near-miscible water-alternating-gas injection performance in water-wet and mixed-wet systems. *SPE J* 18(01):114–123. <https://doi.org/10.2118/145191-PA>
- Fathi E, Akkutlu IY (2014) Multi-component gas transport and adsorption effects during CO₂ injection and enhanced shale gas recovery. *Int J Coal Geol* 123:52–61
- Gamadi TD, Elldakli F, Sheng J (2014) Compositional simulation evaluation of EOR potential in shale oil reservoirs by cyclic natural gas injection. Paper presented at the SPE/AAPG/SEG unconventional resources technology conference. <https://doi.org/10.15530/URTEC-2014-1922690>
- Ghafoori A, Shahbazi K, Darabi A, Soleymanzadeh A, Abedini A (2012) The experimental investigation of nitrogen and carbon dioxide water-alternating-gas injection in a carbonate reservoir. *Pet Sci Technol* 30(11):1071–1081
- Ghorbani M, Mohammadi AH (2017) Effects of temperature, pressure and fluid composition on hydrocarbon gas-oil interfacial tension (IFT): An experimental study using ADSA image analysis of pendant drop test method. *J Mol Liq* 227:318–323
- Harbert L (1983) Low interfacial tension relative permeability. Paper presented at the SPE annual technical conference and exhibition. <https://doi.org/10.2118/12171-MS>
- Hebach A, Oberhof A, Dahmen N, Kögel A, Ederer H, Dinjus E (2002) Interfacial tension at elevated pressures measurements and correlations in the water+ carbon dioxide system. *J Chem Eng Data* 47(6):1540–1546
- Heuer Jr, GJ (1957) Interfacial tension of water against hydrocarbon and other gases and adsorption of methane on solids at reservoir temperatures and pressures. The University of Texas at Austin
- Hocott C (1939) Interfacial tension between water and oil under reservoir conditions. *Trans AIME* 132(01):184–190
- Hoffman BT (2012) Comparison of various gases for enhanced recovery from shale oil reservoirs. Paper presented at the SPE improved oil recovery symposium. <https://doi.org/10.2118/154329-MS>
- Hough E, Rzasa M, Wood B (1951) Interfacial tensions at reservoir pressures and temperatures; apparatus and the water-methane system. *J Petrol Technol* 3(02):57–60
- Jaeger PT (1998) Grenzflächen und Stofftransport in verfahrenstechnischen Prozessen am Beispiel der Hochdruck-Gegenstromfraktionierung mit überkritischem Kohlendioxid: Shaker
- Jahanbakhsh A, Shahverdi H, Fatemi S, Sohrabi M (2018) Gas/oil IFT, three-phase relative permeability and performance of water-alternating-gas (WAG) injections at laboratory scale. *J Oil Gas Petrochem Sci* 1(1):00005
- Jennings HY, Newman GH (1971) The effect of temperature and pressure on the interfacial tension of water against methane-normal decane mixtures. *Soc Petrol Eng J* 11(02):171–175
- Jho C, Nealon D, Shogbola S, King A Jr (1978) Effect of pressure on the surface tension of water: Adsorption of hydrocarbon gases and carbon dioxide on water at temperatures between 0 and 50 C. *J Colloid Interface Sci* 65(1):141–154
- Jin F (2017) Principles of enhanced oil recovery. In: *Physics of petroleum reservoirs*. Springer, pp 465–506
- Jin L, Hawthorne S, Sorensen J, Pekot L, Bosshart N, Gorecki C, Harju J (2017) Utilization of produced gas for improved oil recovery and reduced emissions from the Bakken formation. Paper presented at the SPE health, safety, security, environment, and social responsibility conference-North America. <https://doi.org/10.2118/184414-MS>
- Jin L, Hawthorne S, Sorensen J, Pekot L, Kurz B, Smith S, Dalkhaa C (2017) Extraction of oil from the Bakken shales with supercritical CO₂. Paper presented at the SPE/AAPG/SEG unconventional resources technology conference. <https://doi.org/10.15530/URTEC-2017-2671596>
- Karimaie H, Lindeberg EG, Torsaeter O, Darvish GR (2007) Experimental investigation of secondary and tertiary gas injection in fractured carbonate rock. Paper presented at the EUROPEC/EAGE conference and exhibition
- Kashefi K (2012) Measurement and modelling of interfacial tension and viscosity of reservoir fluids. Heriot-Watt University, New York
- Kashefi K, Pereira LM, Chapoy A, Burgass R, Tohidi B (2016) Measurement and modelling of interfacial tension in methane/water and methane/brine systems at reservoir conditions. *Fluid Phase Equilib* 409:301–311
- Kulkarni MM, Rao DN (2005) Experimental investigation of miscible and immiscible water-alternating-gas (WAG) process performance. *J Petrol Sci Eng* 48(1–2):1–20
- Lepski B (1997) Gravity-assisted tertiary gas injection process in water-drive oil reservoirs. Louisiana State University and Agricultural and Mechanical College, New York

- Li L, Sheng JJ (2017) Upscale methodology for gas huff-n-puff process in shale oil reservoirs. *J Petrol Sci Eng* 153:36–46
- Massoudi R, King A (1975) Effect of pressure on the surface tension of aqueous solutions. Adsorption of hydrocarbon gases, carbon dioxide, and nitrous oxide on aqueous solutions of sodium chloride and tetrabutylammonium bromide at 25. deg. *J Phys Chem* 79(16):1670–1675
- Mehrjoo H, Riazi M, Amar MN, Hemmati-Sarapardeh A (2020) Modeling interfacial tension of methane-brine systems at high pressure and high salinity conditions. *J Taiwan Inst Chem Eng* 114:125–141
- Meng X, Sheng JJ, Yu Y (2017) Experimental and numerical study of enhanced condensate recovery by gas injection in shale gas-condensate reservoirs. *SPE Reservoir Eval Eng* 20(02):471–477. <https://doi.org/10.2118/183645-PA>
- Mu L, Liao X, Chen Z, Zou J, Chu H, Li R (2019) Analytical solution of Buckley–Leverett equation for gas flooding including the effect of miscibility with constant-pressure boundary. *Energy Explor Exploit* 37(3):960–991
- Ramey Jr, H (1973) Correlations of surface and interfacial tensions of reservoir fluids. Society of Petroleum Engineers
- Ren Q-Y, Chen G-J, Yan W, Guo T-M (2000) Interfacial tension of (CO₂+ CH₄)+ water from 298 K to 373 K and pressures up to 30 MPa. *J Chem Eng Data* 45(4):610–612
- Rushing JA, Newsham KE, Van Fraassen KC, Mehta SA, Moore GR (2008) Laboratory measurements of gas-water interfacial tension at HP/HT reservoir conditions. Paper presented at the CIPC/SPE gas technology symposium 2008 joint conference. <https://doi.org/10.2118/114516-MS>
- Sachs W, Meyn V (1995) Pressure and temperature dependence of the surface tension in the system natural gas/water principles of investigation and the first precise experimental data for pure methane/water at 25 C up to 46.8 MPa. *Colloids Surf A Physicochem Eng Aspects* 94(23):291–301
- Sanchez-Rivera D, Mohanty K, Balhoff M (2015) Reservoir simulation and optimization of Huff-and-Puff operations in the Bakken Shale. *Fuel* 147:82–94
- Shahrokhi O, Sohrabi M, Masalmeh S (2018) The impact of gas/oil IFT and gas type on the performance of gas, WAG and SWAG injection schemes in carbonates rocks. Paper presented at the SPE EOR conference at oil and gas West Asia. <https://doi.org/10.2118/190338-MS>
- Shariat A (2014) Measurement and modeling gas-water interfacial tension at high pressure/high temperature conditions
- Sheng JJ, Chen K (2014) Evaluation of the EOR potential of gas and water injection in shale oil reservoirs. *J Unconv Oil Gas Resour* 5:1–9
- Sohrabi M, Fatemi SM (2012) Experimental investigation of oil recovery by different injection scenarios under low oil/gas IFT and mixed-wet condition: water-flood, gas injection, WAG and SWAG injection. Paper presented at the Abu Dhabi International Petroleum Conference and Exhibition
- Standing M (1947) A pressure-volume-temperature correlation for mixtures of California oils and gases. Paper presented at the Drilling and Production Practice
- Sun J, Zou A, Sotelo E, Schechter D (2016) Numerical simulation of CO₂ huff-n-puff in complex fracture networks of unconventional liquid reservoirs. *J Nat Gas Sci Eng* 31:481–492
- Sutjiadi-Sia Y, Jaeger P, Eggers R (2008) Interfacial phenomena of aqueous systems in dense carbon dioxide. *J Supercrit Fluids* 46(3):272–279
- Sutton R (1985) Compressibility factors for high-molecular-weight reservoir gases. Paper presented at the SPE annual technical conference and exhibition. <https://doi.org/10.2118/14265-MS>
- Tewes F, Boury F (2004) Thermodynamic and dynamic interfacial properties of binary carbon dioxide–water systems. *J Phys Chem B* 108(7):2405–2412
- Todd M, Longstaff W (1972) The development, testing, and application of a numerical simulator for predicting miscible flood performance. *J Petrol Technol* 24(07):874–882
- Wiegand G, Franck E (1994) Interfacial tension between water and non-polar fluids up to 473 K and 2800 bar. *Ber Bunsenges Phys Chem* 98(6):809–817
- Wu Z, Liu H, Pang Z, Wu C, Gao M (2016) Pore-scale experiment on blocking characteristics and EOR mechanisms of nitrogen foam for heavy oil: a 2D visualized study. *Energy Fuels* 30(11):9106–9113
- Wu Z, Huiqing L, Wang X, Zhang Z (2018) Emulsification and improved oil recovery with viscosity reducer during steam injection process for heavy oil. *J Ind Eng Chem* 61:348–355
- Yang D, Tontiwachwuthikul P, Gu Y (2005) Interfacial interactions between reservoir brine and CO₂ at high pressures and elevated temperatures. *Energy Fuels* 19(1):216–223
- Yiling T, Yanfan X, Hongxu Z, Xi-Jing D, Xiao-Wen R, Feng-Cai Z (1997) Interfacial tensions between water and non-polar fluids at high pressures and high temperatures. *Acta Phys Chim Sin* 13(1):89–95
- Yu W, Lashgari HR, Wu K, Sepehrnoori K (2015) CO₂ injection for enhanced oil recovery in Bakken tight oil reservoirs. *Fuel* 159:354–363
- Yu Y, Li L, Sheng JJ (2017) A comparative experimental study of gas injection in shale plugs by flooding and huff-n-puff processes. *J Nat Gas Sci Eng* 38:195–202
- Zhao G-Y, Yan W, Chen G-j (2002) Measurement and calculation of high-pressure interfacial tension of methane+ nitrogen/water system. *J Univ Petrol China Nat Sci Ed* 26(1; ISSU 129):75–78

Publisher's Note Springer Nature remains neutral with regard to jurisdictional claims in published maps and institutional affiliations.